ISSN 0252-1075
Contribution from IITM
Research Report No. RR-103

Interannual Variability of Kelvin and Rossby Waves in the Indian Ocean from Topex / Poseidon Altimetry Data

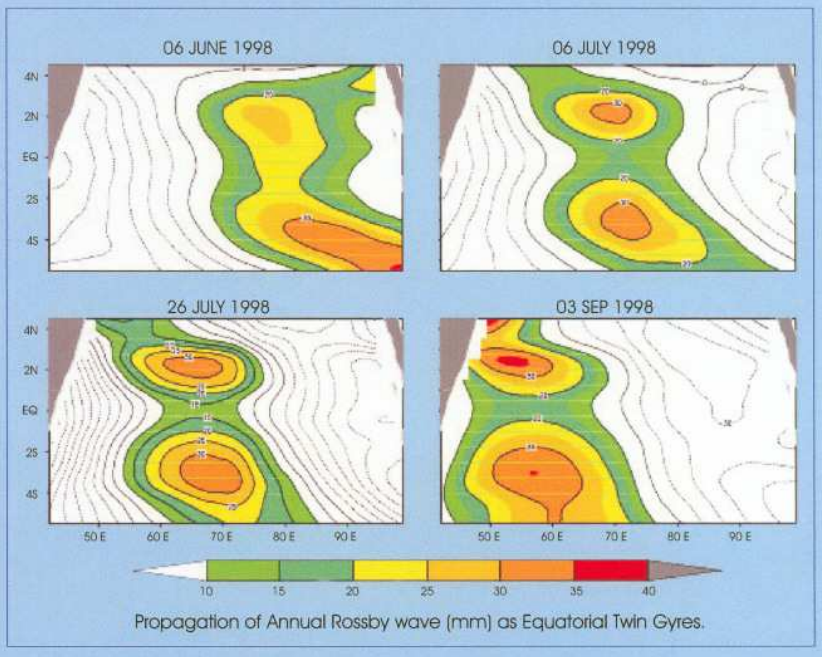

Propagation of Annual Rossby wave (mm) as Equatorial Twin Gyres.

C. Gnanaseelan, B.H. Vaid, Paulo S. Polito
and
P.S. Salvekar

March 2004

Indian Institute of Tropical Meteorology
Pune - 411 008, India

ISSN 0252-1075
Contribution from IITM
Research Report No. RR-103

Interannual Variability of Kelvin and Rossby Waves in the Indian Ocean from Topex / Poseidon Altimetry Data

C. Gnanaseelan, B.H. Vaid, Paulo S. Polito
and
P.S. Salvekar

March 2004

Indian Institute of Tropical Meteorology
Dr. Homi Bhabha Road, Pashan Pune - 411 008
Maharashtra, India

E-mail : lip@tropmet.ernet.in
Web : http://www.tropmet.ernet.in
Fax : 91-020-25893825
Telephone : 91-020-25893600

CONTENTS

Interannual Variability Of Kelvin And Rossby Waves In The Indian Ocean From Topex/Poseidon Altimetry Data

C. Gnanaseelan, B. H. Vaid, Paulo S Polito and P. S. Salvekar*

Abstract

Sea Surface Height Anomalies (SSHA) over the Indian Ocean acquired by the Topex/Poseidon (T/P) satellite from 1992-2002 are decomposed using two dimensional Finite Impulse Response Filter. The filtered signal components are basin scale seasonal waves, westward propagating Rossby waves, eastward propagating Kelvin waves, mesoscale eddies and small scale residuals. In this study emphasis has been given to only Kelvin and Rossby wave components. It has been seen that sum of these components does not depart significantly from the original SSHA signal. Kelvin and Rossby wave components are of main interest because they are associated with energy transfer among the oceanic basin. Its manifestation might appear as slight rising of the mean sea surface height by few centimeters. Westward traveling Rossby waves radiated from the western side of the Indian subcontinent are found to be the main source for the seasonal fluctuations between 6° and 10° N in the western Arabian Sea region (off Somalia). Semi annual and annual Rossby waves propagating from the southern tip of Indian subcontinent are found to reach the western end of the Arabian Sea around March and August respectively in every years. Phase speeds of the different components (biannual, annual and semi annual Rossby waves and tropical instability waves etc.) at different latitudes are calculated and their variability is studied. Time period amplitude and wavelength of different components of Rossby waves and Kelvin waves are studied. Total time taken by different components of the Rossby waves for crossing the equatorial belt and for some other latitudinal belt of Indian Ocean are also examined. Kelvin wave propagation and reflection from the east near the Sumatra coast is clearly seen in the analysis. It is also seen that the reflected Kelvin wave mainly splits up into three major components: one travelling westward as equatorial Rossby waves, one travelling northward along the perimeter of Bay of Bengal as coastally traped Kelvin waves and one travelling southward. Interannual variability in the SSHA and the Rossby and the Kelvin wave component are examined in detail. Hovmoller diagrams are analyzed to clearly understand the propagation of the Rossby and the Kelvin wave components and its variability.

---

* Earth Observation Department, National Institute of Space Research, Brazil.

INTRODUCTION

This report is focused mainly on planetary waves and their propagation in the Indian Ocean that has direct influence to the regional (Indian) monsoon climate. It is particularly focused on the role which satellite remote sensing (Topex/Poseidon satellite data is used here) play in identifying and understanding the mechanisms of these processes. It has been seen that cross equatorial winds over the Indian Ocean mainly during the month of April and May causes a change in the upper ocean, depressions in the thermocline along with a rise in the ocean surface, which propagates eastward along the equator as downwelling Kelvin waves (McCreary et al., 1993). These downwelling Kelvin waves are mainly triggered by the monsoon winds. The necessary condition for the propagation of Kelvin waves is that the horizontal pressure gradient force and Coriolis force act in opposite direction. For example if a parcel of water is moving northwards in the Northern Hemisphere (NH), with a coastal boundary on its right, the Coriolis force acts to reflect the parcel to the right, but beyond a limited extent this is impossible because the coastal boundary is in the way. Water piles up against the boundary, giving rise to an offshore horizontal pressure gradient force; this keeps the parcel of the water moving parallel to the coast. As a result the coast may act as wave guides to the perturbations known as coastal Kelvin waves, which can travel as surface (barotropic) waves or baroclinic waves.

A Kelvin wave may be regarded as a coastally trapped wave within a certain distance of the coast, because outside that distance its amplitude decays so as to be hardly discernible. This distance is known as the Rossby radius of deformation (L) and can be calculated from L=c/f; where f is Coriolis parameter and c is wave speed. Along the equator Coriolis force (f) is zero, hence the equator also serves as a wave guide. An equatorial Kelvin wave is two parallel coastal Kelvin waves propagating with the boundary on the right in the NH and left in the SH. As a result Kelvin waves can only propagate eastwards along the equator. The surface equatorial Kelvin wave travels very fast at about 200-300 cm/s (Gill, 1982) and their Rossby radius of deformation can be about 2000 km. The baroclinic Rossby radius of deformation is associated with the normal modes. The baroclinic mode has an associated Rossby radius $a_n=c_n/|f|$, (where n= 1, 2, 3.....and c_n are baroclinic phase speeds). The typical values of the baroclinic Rossby radius are 10-30 km, with larger values in low latitudes. As equatorial zone acts as a wave guide, the equator also serves as a Kelvin wave boundary. Because the Coriolis force acts cumsole, the equatorial Kelvin waves can only travel eastwards in both hemispheres, having maximum amplitude at the equator, and amplitude decreasing exponentially further north or south of the equator. While the Kelvin wave progresses, the maximum amplitude is always on the right (left) in the NH (SH). In a closed basin Kelvin waves travel counterclockwise in the NH and clockwise in the SH.

The first mode baroclinic Kelvin wave has a moderate speed of 250 cm/s (McCreary et al., 1993), and takes about 30 days to travel from the western boundary to the eastern boundary (40°-100°E) in the Indian Ocean. One of the most interesting aspects of the equatorial Kelvin waves in the Indian Ocean is that on reaching the eastern boundary, some of the energy moves along the coasts as two coastal Kelvin waves, one northward and the other southward and some reflect as westward propagating Rossby waves. Recent model results (Potemra et al., 1991; Yu et al., 1991; McCreary et al., 1993, Gnanaseelan et.

al. 2003) showed that the coastally trapped Kelvin waves travel along the rim of the Bay of Bengal. Also the Rossby waves generated at the southern tip of India and Sri Lanka propagate westward in the Arabian Sea, the recent studies found that it has a strong relation with Arabian Sea warm pool (Shenoi et. al. 1999). Also it has been observed that Rossby waves are generated along the eastern boundary of the Bay of Bengal by local winds or the equatorial Kelvin waves impinging on the eastern boundary.

A new theory which has evolved from results of numerical experiments (Potemra et al., 1991; McCreary et al., 1993) is that the subsurface reversal of the currents in the eastern Arabian Sea is largely the result of the Rossby waves radiated by Kelvin waves propagating along the west coast of India. So the numerical experiments raise the possibility that the coastal circulation along the west coast of India and annual cycle of currents over the Arabian Sea are mainly influenced by the events in the Bay of Bengal. From the synergistic observations of Rossby waves it has been concluded that when a small region of the ocean responds to a sharp change in conditions (e.g. a rapid change in current direction or additional wind stress) the system is disturbed locally. If the response has involved a latitudinal displacement of a parcel of water, then potential vorticity (akin to the parcel's angular momentum about the Earth's axis) provides a restoring force. Since the restoring force is proportional to the displacement the result is a sinusoidal signal, an intriguing property of which is that the propagation is westward although the displacements are meridional (see Fig.1.1).

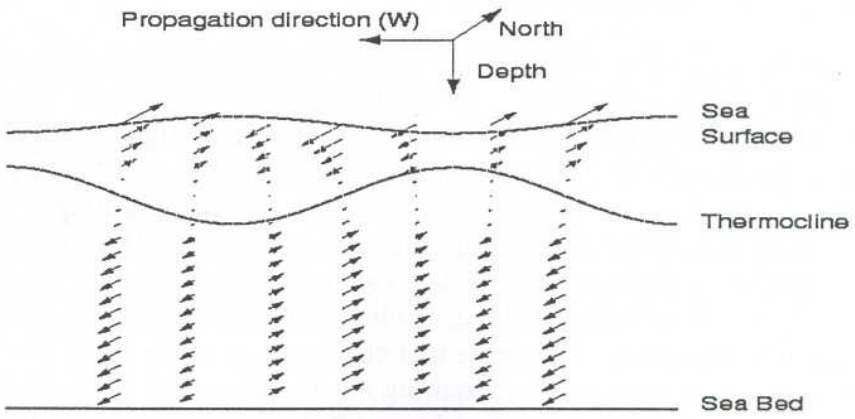

Fig. 1.1 A schematic of the depth structure of a first-order baroclinic Rossby wave, with a rise in the sea surface of a few centimeters being mirrored at the thermocline by a depression of tens of meters. The meridional velocities change sign about the thermocline (Source: Quartly et al. 2000).

These Rossby waves are the large scale dynamical response of the ocean to wind forcing and buoyancy forcing (heating and cooling) at the eastern boundaries and the ocean interior. They can also be generated by perturbations along the eastern boundaries associated with coastally trapped waves originating at low latitudes (White, 1985). The Rossby waves or planetary waves arise from the need for potential vorticity conservation. Oceanic Rossby waves (otherwise called 'planetary waves') are large-scale propagating features that owe their nature to being in a fluid co-rotating with the solid earth. Their surface manifestation might appear as slight rising of the mean sea surface height (SSH) by a few centimeters and an increase in sea surface temperature (SST) by a fraction of a

degree. Rossby waves travel westward at speeds of the order of 1 to 10 km/day or 1.16 to 11.57 cm/s (the speed increases equatorward) carrying information from their source region, and they set the response time of processes in the west of basins to changes occurring in the east. Possible stimuli include strong changes in wind forcing, variations in current and the passage of poleward-propagating Kelvin waves. The resultant baroclinic Rossby waves have a velocity structure in the meridional direction, and change the height of the thermocline by tens of meters. Their effect on reaching the west is to intensify the western boundary current, and possibly to alter its position and thus change the ocean's modification of the atmosphere (Jacobs et al. 1994).

To understand better the complex ocean-atmosphere coupled system, and especially the likelihood of significant climate change, one needs a good understanding of Rossby waves - where they occur, their amplitude, and particularly their speed of propagation, which determines the timescale for ocean-atmosphere feedback. Rossby waves move slowly, at typical speeds of a few centimetres per second. These waves have periods longer than a day and some Rossby waves travel very slowly taking months to years to cross the ocean basin. Rossby waves propagate zonally, along the equator, but also along other latitudes. Another important characteristic of these Rossby waves is that these waves carry energy from the ocean interior to the western boundary region. Rossby waves significantly shorten their wavelengths after reflection from the western edge of the ocean basin, and lengthen their wavelengths after reflection from the eastern edge. These waves are abruptly amplified by the major topographic features. (Hill, K.L. et. al. 2000)

Rossby waves play a critical role in the transient adjustment of ocean circulation to changes in large-scale atmospheric forcing. Rossby waves have been much more difficult to detect in the oceans because of their small sea surface signature (height variation of order of 10 cm or smaller), slow propagation speeds (of order of 10 cm/s or less), and long wavelengths (hundreds to thousand km). The lowest order (barotropic) Rossby wave is uniform vertically, independent of stratification, and propagates across an entire ocean basin in a period of about a week. This is too fast to be resolved by an orbiting satellite. The next higher order (first baroclinic) mode is surface intensified, and depends strongly on stratification, has a velocity profile that changes sign at the depth of the thermocline , and propagates much more slowly, requiring months to decades to cross an ocean basin. In general it has been concluded that Rossby and Kelvin waves affect the thermocline depth, and hence the ocean's temperature profile, as well as the sea surface height. The waves can either raise or lower the thermocline, leading to a decrease or increase respectively in the sea surface height.

A lowering of the thermocline leads to a warming effect in the region of the disturbance, since the cooler water under the thermocline is forced down and replaced by warmer water. The opposite is true for a rising of the thermocline i.e. there is a cooling associated with an upwelling event. For the first-baroclinic mode, variations in sea surface height are inversely mirrored in the thermocline depth, with approximately three orders of magnitude greater amplitude (Gill 1982). A one centimeter sea level rise will thus correspond to a ten meters thermocline depression, and a significant variation in the upper-ocean thermal structure. The basin crossing time increases with increasing latitude because of the latitudinal variation in phase speed owing to the β-effect. As a result the crests and troughs of the Rossby waves initiated simultaneously along the entire eastern boundary of

an ocean basin arrive at western boundary much sooner at lower latitudes than at higher latitudes, an effect often referred to as β-refraction. In most regions of the ocean, it is generally believed that slower, higher order baroclinic Rossby wave modes play a lesser role in large-scale circulation dynamics. The advent of satellite altimetry (here in this study TOPEX/POSEIDON (T/P) altimetry) opened a new era for detection of these Rossby waves (Chelton and Schlax, 1996).

The phase speeds depend inversely on the square of the Coriolis parameter, and waves take only months to cross an ocean basin such as Indian Ocean in low latitudes and years to decades at higher latitudes. The vertical structure of these waves becomes progressively more complicated as the mode increases, while the phase speed decreases. It also plays a vital role in the surface circulation and currents. Kelvin and Rossby waves are of interest because of their main mechanism of energy transfer properties. And this is found to have great impact on the eddies formation and other oceanic processes which directly or indirectly affecting the monsoon. It is also found that the seasonal eddies forming in the Arabian Sea have a strong relation with the equatorial Rossby waves and the reflected waves from the west coast of India.

METHODOLOGY

Finite Impulse Response (FIR) filter

Finite impulse response (FIR) filter is the band pass filtering technique for filtering the SSHA into several spectral bands. These bands include propagating (Rossby, Kelvin, and tropical instability waves) and non propagating (annual and interannual basin-scale variability and eddies) signals. These signals are decomposed through a series of finite impulse response band-pass filters (Polito et. al. 2000). Even though the filter can be applied for the globe, present study is concentrated towards the Indian Ocean region only. Phase speed, amplitude, wave length, and time period were calculated for all Kelvin and Rossby wave components using Radon transform procedure based on Polito and Cornillon, (1997).

Data processing and analysis

The T/P data are those distributed by the Jet Propulsion Laboratory Physical Oceanography Distributed Active Archive Center (JPL/PODAAC) published for the World Ocean Circulation Experiment conference (WOCE global data, version 1.1, 1998). The data consist of sea surface height anomalies in relation to a 5-year average (1993-1998) and are presented in bin-averaged grid maps of $0.5^\circ \times 0.5^\circ \times 10$ days. The data cover latitudes between 66°S and 66°N, and from October 1992 to December 2002. All the standard corrections are applied (Benada, 1997).

The sea surface height anomalies (η_o) is bicubically interpolated to a $1^\circ \times 1^\circ$ grid. Maps of $\eta_o(x,y)$ are converted to zonal temporal diagrams of $\eta_o(x,t)$ one for every degree of latitude. Data over shallow areas (depth $H \leq -1000$m), small islands ($x \leq 3^\circ$) and zonally enclosed water bodies are excluded to facilitate filtering. Only continuous open-ocean areas with zonal dimension in excess of 20° wide enough to apply the filter are used. Each

η_o data matrix is decomposed through a 2D zonal-temporal filter. The filters are designed based on previous knowledge of the signal (that is, its approximate period and its phase speed within a factor of two). This information is input as a set of parameters that restricts each filter output to a particular region of the frequency-wave number spectrum.

There are potential problems inherent to the application of 2D FIR filters to T/P data. At locations close to the continental margins the filters operate with less data and thus, are less skilled compared to the open ocean. At high latitudes the wavelengths become comparable to the zonal resolution of T/P making it difficult to resolve its signal. At low latitudes the non-propagating seasonal signal may not be completely distinguished from the fast basin-wide Rossby and Kelvin waves. The band-pass FIR filters have a smooth transition between the pass-band and the stop-bands. Since the bands are relatively wide, a slight contamination between adjacent bands is possible. This problem is minimized by removing the correlated part of each component from all the others.

Tidal aliasing is a potential problem caused by the temporal under sampling of the remainder of the tidal signal left in the T/P record after the model tides are removed. The amplitude of the aliased signal depends on the mismatch between the model and observed tides and is generally small compared to the amplitude of the waves (Schlax and Chelton,1994). Due to the sampling strategy of T/P and to the 2D filter the tidal aliasing problem is minimized, and the only frequency band that can be affected is η_1. In analogy to the tidal aliasing, Rossby (or other) waves can be aliased whenever the wavelength is similar or smaller than twice the track separation (Parke et. al., 1998). The filter for each frequency was limited to a latitudinal band specific to that frequency and basin to avoid spatial aliasing. These latitudinal bands were obtained empirically and are listed in Table B.

FIR formulation

The individual contributions of all the wave components of different periods and characteristics are separated from SSHA signal using two dimensional FIR filters. FIR filters are based on convolution of two sequences, the original data η_o, and the filter f, resulting in the filtered data η_f. In the present case $\eta_o(x,t)$ is a function of longitude and time; therefore the filter f(i,j) is a function of longitudinal lag i and temporal lag j. The filtered matrix $\eta_f(x,t)$ is obtained from

$$\eta_f(x,t) = \sum_{i=-m}^{m}\sum_{j=-n}^{n}\eta_0(x+i,t+j)f(i,j) \quad \ldots\ldots\ldots\ldots\ldots\ldots\ldots\ldots(1)$$

The size of filter is controlled by parameter m and n. The filter is applied to separate the Rossby and Kelvin waves of different periodicity (Polito et. al. 2000).

The filter for the components η_{t1}, η_{t2} and η_E is the Gaussian surface:

$$f(i,j) = \frac{e^{-1/2((\pi i/m)^2+(\pi j/n)^2)}}{N} \qquad \text{.....(2)}$$

$$\text{with N such that } \sum_{i=-m}^{m}\sum_{j=-n}^{n} f(i,j) = 1$$

The size of the filter, controlled by parameters m and n, is set to half-year and twice the basin width for η_{t1}. The filter is initially oversized to minimize the mixing of biannual and annual signals into the non-propagating component η_{t1}. After the Rossby wave signals are removed this filter is resized to 183 days and 15° and applied a second time to yield η_{t2}. These parameters are set to avoid contamination by both Kelvin waves and aliased tidal signals. After the Kelvin wave signal is removed, the filter parameters are set to 50 days and 5° yielding η_E

For the band-pass filtering of the Rossby wave components (η_{24}, η_{12} , η_6 , η_3) and the instability waves (η_1) the filter f(i ,j) is a Gaussian tapered cosinusoidal surface(Polito et. al. 2000)

$$f(i,j) = \frac{e^{-1/2((\pi i/m)^2+(\pi j/n)^2)}}{N}\cos\left(\frac{2\pi i}{L} - \frac{2\pi j}{T}\right) + M, \qquad \text{.....(3)}$$

$$\text{with } M \text{ and } N \text{ such that } \begin{cases} \sum_{i=-m}^{m}\sum_{j=-n}^{n}\left|f(i,j)\right| = 1, \\ \sum_{i=-m}^{m}\sum_{j=-n}^{n} f(i,j) = 0, \end{cases}$$

where L and T are the wavelength and period of the approximate center of each pass band. T is set to 730, 365, 183, 91, and 45 days and L is such that $L = CpT$. The filter size parameters m and n are set to one period and one wavelength. The Gaussian part of Equation (3) works as a smoother while the cosine part limits the power of the response to a specific area in the 2D spectrum. This can be understood as a 2D version of the tapered cosine window functions (Blackman, Hamming, Hanning, etc.) used in classical 1D spectral analysis, whose main advantages are the same: to minimize phase distortion and to reduce the amplitude of side-lobes (leaking).

For the band-pass filtering of η_K the filter f(i, j) is composed of the positive elements of f in (3), with M and N such that

$$\sum_{i=-m}^{m}\sum_{j=-n}^{n} f(i,j) = 1$$

When filtering for η_K, T is set to 45 days and it is only applied between 5.5°S and 5.5°N, before filtering for η_E. This filter has a much broader pass band than those used for the Rossby wave components. This choice was taken because the eastward propagating signals are not as regular in period and wavelength as their westward counterparts.

An initial guess (indicated by the subscript 1) for the average zonal phase speed, Cp_1 as a function of latitude, is used to obtain L_1 from $L_1 = Cp_1 T_1$ with $T_1 = 730$, 365, 183, 91 and 45 days. The components of η_0 are filtered in the following order: η_{t1}, η_{24}, η_{12}, η_6, η_1, η_{t2}, η_K and η_E. Each band-passed signal is removed from the original data at every step before the next filter is applied, for example: η_{24} is obtained by filtering $\eta_0 - \eta_{t1}$; η_{12} is obtained by filtering $\eta_o - \eta_{t1} - \eta_{24}$; η_6 is obtained by filtering $\eta_o - \eta_{t1} - \eta_{24} - \eta_{12}$; and so forth.

After the filter is applied to obtain each component, the filtered signal is multiplied by a constant factor g such that the variance of $\eta - g\eta_f$ is minimized. These filters are characterized by a smooth transition between the stop-bands and the pass-band, therefore some contamination among the wave signals can occur. To minimize this problem a fraction g_{ij} of the signal η_i is removed from η_j for all $j \neq i$, g_{ij} is such that the variance of $(\eta_j - g_{ij}\eta_{ij})_{is}$ minimized.

The filters are applied to the $\eta_0(x,t)$ fields at every degree of latitude, using the initial values Cp_1, T_1 and L_1. The same Cp_1 is used for each of the Rossby wave bands. New values for the average Cp, L and T are estimated for each of the bands using a Radon transform procedure based on Polito and Cornillon, (1997). One estimate is made for each area measuring T_1 by L_1 and the estimates are averaged in space and time to obtain a single value of Cp, L and T per latitude. The filtering procedure is then repeated using new parameters (but the same original data) until the average difference between Cp of the last loop and the present value of Cp has converged within 10% of the latter. If during the iterations the filtered signal falls below 10% of the variance of its original signal, the filtered data are flagged and filtered once more with Cp as given by the initial guess. If the period of the filtered signal is within the range of the next band, the filtered data are flagged. If during the iterations the updated value of Cp differs from the initial guess by more than a factor of 2 while the amplitude remains above the 10% threshold, the loop is abandoned and the data are filtered once more with Cp as given by the initial guess and its results are flagged.

RESULTS AND DISCUSSION

The eastward propagation of equatorial Kelvin waves in the Indian Ocean during the monsoon transition periods April – May and October- November plays a vital role in transporting heat and mass in the equatorial region. Recent studies (Saji et. al. 1999, Vinayachandran et. al. 2002, Rao et. al. 2002) have found large interannual variability in the tropical Indian Ocean SST and subsurface temperature. Interannual anomalies in SSH, winds and other surface heat fluxes indicate the importance to understand it very well in the context of air sea interaction processes. The planetary waves such as Rossby and Kelvin waves, its propagation and variability can clearly be seen in the original SSHA. However the present detailed study helped to understand the variability very well. As the

Kelvin wave has a very important role in the Rossby wave formation in the eastern tropical Indian Ocean, it is worth examining its variability. As the SSHA signals are mirror image of the thermocline in the form of deepening or shoaling of thermocline, the study on the variability in SSHA signals and Kelvin or Rossby waves signals infact give a clear picture of the upper ocean heat content variability (Chambers et. al. 1997). Infact the downwelling waves (or +ve SSH anomaly) are found to be coinciding with deeper thermocline and upwelling waves (or –ve SSH anomaly) coincide with shallow thermocline. Figure 1 shows the propagation of fast moving Kelvin wave signals during April – May 1996 and 2002. The Kelvin wave signals are filtered from the observed TOPEX/POSEIDON SSHA. The filtered Kelvin wave signals are mostly confined between 3°S and 3°N as equator acts as a wave guide and in this region the value of the Rossby radius of deformation is found to be very large say 2000kms. The Kelvin wave signals are found to be in the range of 3 to 5 cm with a lot of interannual variability, which is clear from Fig 1(left panels for 1996 and right panels for 2002) and Fig 2. The equatorial Kelvin waves in 2002 are found to be stronger than 1996. More detailed study is required to understand the variability eventhough the present study focuses mainly on IOD years.

Figure 2 shows the longitude – time plot (Hovmoller diagram) of Kelvin wave components along the equator. The summer semi annual Kelvin wave usually starts in April at 44°E and reaches the eastern boundary (96°E) around May - June. Its mean speed is found to be 90.6 Kms/day. Semi annual Kelvin wave is also found to be originating around October-November in the western equatorial Indian Ocean and reaching the eastern boundary (96°E) around November-December. This is mainly due to the abrupt change in wind direction during October and November. As abrupt change in the wind direction across the equatorial region in the month of April and May causes a change in the upper ocean, depressions in the thermocline and rise in the ocean surface, which propagate eastward along the equator as a downwelling Kelvin wave. By this process, Kelvin waves deepen the thermocline in the eastern equatorial Indian Ocean and also cause significantly higher sea level (elevated by 5 – 10 cm; Ali 1993). The semi annual signals are found during the entire period with significant interannual variability. The magnitudes are normally in the range of 3 – 5 cm, exception being in 1995 and 1998, the years following strong IOD events. The signals of 1995 and 1998 are found to be in the range of 5 – 7 cm. As 1997 was a stronger IOD year than 1994, the 1998 Kelvin wave signals are found stronger than 1995. Moreover the exceptional signals in 1995 were weakened its strength and slowed down considerably when it reached about 70°E. The variability found in the strength of the Kelvin wave may be directly related to wind stress curl value. Figure 3 shows the Hovmoller diagram of the TOPEX/POSEIDON SSHA. Sea surface height anomaly along the equator clearly shows the eastward propagation of Kelvin waves (Fig 3.a), but the latitudinal average of SSHA along -2.5°S and 2.5° N has revealed the strong westward propagating Rossby waves and its variability than the eastward propagating Kelvin waves (Fig 3.b). The similar picture with much more significance was seen in the latitudinal average of SSHA along 4.5°S and 4.5°N (Fig 3.c). The features were consistent in every year. Thus it is further evident that Kelvin wave signals are confined to equator only. However the Rossby wave signals are found to be strong near 4° latitudes and weak near the equator. Fig 3.a further shows the interannual variability in the Kelvin wave propagation especially in 1998, the year immediately after the strong IOD year 1997. The strong anomalous Rossby wave propagation in 1997 is also clearly seen in the original SSHA signal.

The eastward propagating Kelvin waves after reaching the eastern boundary (Sumatra coast), propagated as two coastally trapped Kelvin waves, one northward and the other southward. Some of the energy can also reflect back as Rossby wave along the equator. In addition to the reflected Kelvin waves in the eastern boundary, the wind stress curl is also playing an important role in Rossby wave generation and propagation. This was evident when strong Rossby wave signals observed in the east week/weeks before the Kelvin wave reached the eastern boundary (for example in 1998). The westward propagating Rossby waves are found to have different periodicity. The semi annual and annual signals are found to have considerable strength and variability. The propagation of equatorial Rossby waves are seen as twin gyres (one centered in the northern hemisphere and the other in the southern hemisphere). Recently Reddy et. al. (2004) found such eddies in their reduced gravity model. Mostly these gyres are seen symmetric with respect to the equator with considerable interannual variability. The propagation of equatorial semi annual Rossby waves during 1994 and 1997 are shown in Fig.4. The chosen years in Fig 4 are positive IOD years. The northern gyre in 1994 was centered along 5.5°N, however a weak southern gyre was centered along 4°S. In contrast to this during 1997 the northern gyre was centered along 3.5°N and southern gyre was centered along 4.5°S. In Fig 5, the semi annual Rossby waves during the years following the above IOD years are analyzed. In 1995, the northern gyre was centered along 4.5°N and southern gyre was centered along 4.5°S, which means that tropical Rossby waves have a local minimum at equator with symmetric maxima at 4°N and 4°S (Delcroix et. al. 1994, J. P. Boulanger et. al 1995 and Chelton et. al. 1996). The observed westward propagation is therefore much more apparent along 4°N than the equator (Fig. 5). However in 1998 the northern gyre was found along 2.5°N and southern gyre along 4.5°S. The annual Rossby wave propagation in different years are shown in Fig 6 and 7. During the dipole years very slowly propagating south dominant (very weak northern) gyres were observed (Fig 6). The annual gyres during the positive dipole years are found reaching the west end in January next year. In contrast to this in 1995 and 1998 (Fig 7) the annual signals propagated much faster and reached the western end in August itself along with the semi annual Rossby waves.

Another very important interannual signal observed during the positive IOD years is the existence of strong biannual signal centered along 2°S during the positive IOD years (Fig 8, the latitudinal average of biannual signal along 3.5°S to 1.5°N). During the positive IOD years 1994 and 1997 strong biannual signals were found propagating westward. The strong biannual signal (of 2 – 3 cm) originated in the east some time in August 1993 and 1996 but propagate slowly and reaches the western boundary in January 1995 and 1998 respectively. The 1997 signals were stronger than 1994 coinciding with the strength of IOD. The biannual signal of 2 to 3 cm magnitude observed in the dipole years may be very important in view of the interannual variability in the region such as IOD and its evolution. Further detailed study is required to understand more about this.

Fig 9 is the Hovmoller diagram of annual and semi annual Rossby waves over 4.5°S to 4.5°N. Phase speed and time taken by the different component of Rossby waves to cross the longitudinal distance at different latitude is given in Table A. For example the annual Rossby wave at 5.5°N and 5.5°S are found to travel at a mean phase speed of 30.55 kms/day and 22.55 kms/day(see Table A) respectively. However some discrepancy has been found in the values of phase speed. Measurement error which leads to discrepancy in phase speed, time period, amplitude and wavelength associated with the data shown in Fig. 15 and Table A is well explained in Polito et.al. 2003 The annual Rossby waves and

semi annual Rossby waves are found to cross 49.5-76.5°E distance in about 100 days and 68 days (see Table A) respectively. It is clear from Table A at 12.5° N that the annual Rossby wave component is reaching the western boundary in 295 days where as at 12.5°S it is taking 434 days. This strongly suggests that the southern Indian Ocean Rossby wave is taking more time to reach western end of the Indian Ocean. Large interannual variability is clearly seen in both the annual and semi annual signals. During the dipole year 1997, strong westward propagating (slowly compared to other years except 1994) anomalous annual Rossby waves were observed which started from eastern boundary in June and reaches western boundary by March 1998 (Fig 9.a), however the strong anomalous semi annual signal reaches western boundary by September 1997 itself (Fig 9.b). Even though the signals were weaker than 1997, the annual signals of 1994 also found propagating slowly and reaching the western boundary by March 1995 only (Fig 9.a).

Figure 10 shows the propagation of annual Rossby wave propagation in the entire north Indian Ocean upto 25°S. Very strong annual Rossby wave signals are observed along 8.5°S latitude, which is found propagating from the west Pacific in January through the Indonesian through flow region. Even though the propagation is shown for only 2000, the picture is similar for other years also. It is also known that the coastal Kelvin waves generated during the north east monsoon period propagate along the east coast of India and reach the southern tip of India in November or December of every year. After reaching the southern tip, a part of it travels northward along the west coast of Indian subcontinent as coastal Kelvin waves (or annual Rossby waves as it has similar features of annual Rossby waves) and other moves westward from southern tip as Rossby waves. The annual Rossby waves component along 10-15°N is found propagating westward from the west coast of India in March and reaches the western end in November or December. Also the annual Rossby waves [period of which at 8.5°N is about 235 days (see Table A)] propagates northward along the west coast of India upto 12° to 13°N and then propagates westward towards the African coast. It is seen that wave components travelling northward along the west coast of India contributing about 15 cm sea level high during December to June, which can not be neglected in the coastal region (west coast of India) where the tidal range is about 1m only. This is the case in the Kerala coast. It is clear from this figure that the annual Rossby wave components reaches the west coast of the Arabian Sea around July - August. Thus annual Rossby wave components are found to be propagating along the west coast upto 13°N and contributing to the sea level rise over the west coast of India. Figure 12 is the T/P SSH anomalies during January to August 2002, which clearly shows that the annual and semi annual Rossby wave signals completely dominated during the period.

Stronger annual Rossby waves during 1995 and 1998 (years following strong positive dipole years) were observed at 8.5°S (Fig 11.a). The semi annual Rossby wave signals at 8.5°S (Fig 11. b) are found to be quite interesting, because out of the two recent positive IOD years, 1994 had very strong signals however 1997 did not have. Considering the disparities in 1994 and 1997 semiannual Rossby waves signals, we explored the possibility of getting the signals from the original Topex SSHA. The time longitude plots of SSHA along the latitudinal average sections (10.5° N and 14.5° N in the fig 12.a and 7.5°S to 12.5° S in Fig 12.b) were analyzed to get the signatures of interannual variability. It is found that the annual Rossby waves signals were seen both in the northern and southern part of the sections, however large interannual variability is found only in the southern counter part. The strong signals extending upto the western boundary (Fig 12.b) is

observed in 1994 and 1997 (the positive dipole years). However the strong westward propagating signals observed every years in the eastern boundary is found to be weakening near 75°E.

Time series of semi annual and annual Rossby wave signals at different points in the equatorial Indian Ocean were analyzed to understand the variability in speed and magnitude during 1994 and 1998. In Fig 13.a (i), the blue lines is the time series of the wave at 90° E, 0.5°N, black line is at 70°E, 0.5° N and red line is at 50°E, 0.5°N. Similarly the time series of speed and magnitude (in mm) are seen at the latitudes 2.5°N and 2.5°S. Figure 13 strongly confirm that the linear theory will fail to explain the sort of changes happening in the planetary wave propagation in the equatorial Indian Ocean.

It is understood in great detail that the seasonal fluctuation in the Arabian Sea SSHA is associated with the seasonal wind reversal (Bruce et. al. 1998). The time period in Fig 14 is chosen in such a way that the seasonal fluctuation of the sea surface height over the Arabian Sea is its peak. It is also important to note that the sea level changes in this period are very much associated with the seasonal monsoon winds and so it has a direct or indirect influence on the Indian monsoon. In this context it is important to study the origin of these sea level anomalies which are found to appear and influence the Arabian Sea. The T/P altimetry data is very useful and a reliable parameter to study those in detail. Apart from the changes in the Arabian see it is understood from the available literature that the Kelvin and Rossby waves play an important role in transporting heat from the western and the eastern equatorial Indian Ocean respectively.

Left panels of Fig 14(a) and 14(b) show the sea level anomalies, middle panels show the semi annual Rossby waves and right panels show the annual Rossby wave components of 1993. It is clear from right panel of Fig 14(a) and 14(b) that the annual Rossby wave components are dominating the semi annual Rossby wave components. It is found that in the eastern equatorial Indian Ocean, the dominance is due to annual Rossby wave component and also in the southern Indian Ocean mainly in the region 60° E to 80°E, 9°S to 15°S also the annual Rossby wave is dominating the semiannual Rossby wave component. However the westward propagating semiannual Rossby wave component in the equatorial Indian Ocean plays a lead role in strengthening the eddies usually formed in the western Arabian Sea. Strong seasonal fluctuations of sea level were found between 4°N and 10° N. It is found mainly due to Rossby wave components radiated from the western side of the Indian subcontinent and it is continuously forced by the action of wind stress curl over the central Arabian Sea (Peter Brandt 2002). In Fig14(a), it can be clearly seen that when the semi annual Rossby waves at 8.5°N (plots 1 of the central panel of Fig14(a)) reaches at the western boundary, the sea level height anomaly signals start strengthening (top one in the left panel of Fig14(a)) between 4°N and 10°N, and as it advances to the western boundary [central panel of Fig 14(a) and 14(b)] the sea level height anomaly signals appear to have high values [left panels of Fig14(a) and 14(b)]. These seasonal fluctuations are found in the monsoon months. And also it has been found that these seasonal fluctuations vary in their strength from year to year. It may be due to the fact that the Rossby waves are strong enough to strengthen the seasonal fluctuation observed in the Arabian Sea.

Figure 15 shows variation of phase speed, time period, wavelength and amplitude of the Rossby wave components with latitudes. It is clear from the phase speed variation of Rossby wave components that the phase speed mainly increases towards the equator. Phase

speed of the Rossby wave component in northern hemisphere is mainly found higher than that of southern counterpart. For example - annual and semiannual Rossby wave mean phase speed at 8.5°N is 23.71 kms/day and 31.91 kms/day (see Table A also) respectively and at 8.5°S it is 18.95 kms/day and 12.27 kms/day (see Table A also).

Conclusion

The results obtained from the Topex/Poseidon altimetry record help to identify the rapid change in surface slope caused by the eastward propagating equatorial Kelvin waves (downwelling and upwelling). The semi annual Kelvin waves are found to be propagating in April – May and October – November in every years with considerable interannual variability. The Kelvin wave components were found strong along the equator. However the equatorial Rossby waves were found strong along 4° latitudes than along the equator. Considerable interannual variability in the equatorial annual and semi annual Rossby waves and annual Rossby waves along 8.5°S were observed especially during the positive Indian Ocean Dipole years. The annual Rossby waves along 7.5°S to 12.5° S were found propagating from the west Pacific. The annual and semi annual Rossby wave signals were found travelling as equatorial twin gyres with strong interannual variability. Strong biannual Rossby wave signals along the equatorial Indian Ocean (south dominant) were observed during the positive IOD years. Rossby waves play an important role in the interannual variability in the tropical Indian Ocean, such as Indian Ocean Dipole. Also Rossby waves are found to be contributing energy to the formation of Great Whirl (GW) in the Somali coast. In spite of their small surface signature, Rossby waves are clearly detected by SSHA and its filtered components. It has been found that Rossby waves and Kelvin waves have variability in different temporal and spatial scale and have significant inter annual variability. The Rossby waves were found playing a very important role in the oceanic processes. Strong seasonal fluctuation has been found in the west coast of Arabian Sea and is found mainly due to the Rossby waves. The inter annual variability in the Planetary (Kelvin and Rossby) waves have been found to be influencing Indian Ocean Dipole.

Acknowledgement

We thank Director, IITM for providing the infrastructure required for the study. The financial support was provided by Department of Ocean Development, Govt. of India through DOD - INDOMOD) project. The authors are thankful to the T/P team and AVISO altimetry for provision of altimeter data. Authors acknowledge Dr. D. Sengupta, IISc, Bangalore for scientific discussion. The authors acknowledge A.K. Mishra, Bijoy Thompson and J. S. Chowdary for their help during the preparation of the report. Dr. A. K. Sahai had critically reviewed the manuscript.

REFERENCES

Ali, M. M., Interface of the reversal of the mixed layer zonal slope along the equatorial Indian Ocean using Geosat altimetry data, International Journal of Remote Sensing, 14, 2,043 – 2,049, 1993.

Benadra, R., Topex/Poseidon Merged GDR generation Buser's handbook, JPL Rep. D - 11007, Jet propul. Lab. Pasadena, Calif., 1997.

Boulanger, J.-P. and Menkes, Propagation and reflection of long equatorial waves in the Pacific Ocean during the 1992- 1993 El- Nino', J. Geophys. Res., 100, 25,041-25,059, 1995.

Boulanger, J.-P., L.L Fu, Evidence of boundary reflection of Kelvin and first-mode Rossby waves from TOPEX/POSEIDON sea level data, J. Geophys. Res., 101, 16, 361-16, 371, 1996.

Brandt, P., Lothar Strammer, Friedrich Schott, Jurgen Fischer, Marcus Dengler, Detlef Quadfasel, Annual Rossby waves in the Arbian Sea from Topex/Poseidon altimeter and insitu data, Deep-Sea Research-II, 49, 1,197-1,210, 2002.

Bruce, J.G., J.C. Kindle, L.H. Kantha, J.L. Kerling, and J.F. Bailey, Recent observations and modelling in the Arabian Sea Laccadive High region, J. Geophys. Res., 103, 7,593-7,600, 1998.

Chelton, D.B., and M.G. Schlax, Global observations of Rossby waves, Science, 272, 234-238, 1996.

Cipollini, P., D. Cromwell, and G. D. Quartly, Variability of Rossby wave propagation in the North Atlantic from TOPEX/POSEIDON altimetry, Proc. IGARSS'96, Lincoln, Nebraska, vol. I, 91-93, 1996.

Chambers D. P. and B. D. Taplay, Long -period ocean heat storage rates and basin scale heat fluxes from Topex, J. Geophys. Res., 102, 10525-10533, 1997.

Clarke, A.J. and X. Liu, Interannual sea level in the northern and eastern Indian Ocean', *J. Phys. Oceanog.*, 24, 1,224-1,235, 1994.

Delcroix T., J. Picaut, G. Eldin, Equatorial Kelvin and Rossby waves evidenced in the Pacific Ocean through Geosat sea level and surface current anomalies, J. Geophys. Res., 96, 3249- 3262, 1991.

Delcroix T., J. P. Boulanger, F. Masia, Geosat – derived sea level and surface current anomalies in the equatorial Pacific during the 1986 – 1989 El-nino and La- nina, J. Geophys. Res., 99, 25,093- 25,102, 1994.

Gill, A.E., Atmosphere Ocean Dynamics, 622pp., Academic Press, San Diego, California, 1982.

Gnanaseelan, C., Bijoy Thompson, A.K. Mishra, B. H. Vaid and P. S. Salvekar, Effect of open ocean circulation on the coastal sea level over the west coast of India', Proceeding of national conference HYDRO- 2003, pp.247-253, 2003.

Hill, K.L., I.S. Robinson and P. Cipollini, Propagation characteristics of extratropical planetary waves observed in the global ATSR sea surface temperature record, *J. Geophys. Res.*, vol. 105, pp. 2,1927-2,1946, 2000.

Jacobs, G. A. and W. J. Emery, Rossby waves in the Pacific Ocean extracted from Geosat altimeter data, American Meteorological Society, 1,155-1,175, 1993.

Killworth, P.D., D.B. Chelton and R. de Szoeke, The speed of observed and theoretical long extra-tropical planetary waves, *J. Phys. Oceanogr.*, 27, 1946-1966, 1997.

McCreary, J. P., W. Han, D. Shankar, and S. R. Shetye, Dynamics of the east India coastal current by Numericals solutions. J. Geophys. Res., 101, 13993-140101996 .

McCreary, J. P., P. K. Kandu, and R. L. Molinari, A numerical investigation of dynamics, thermodynamics, and mixed layer processes in the indian ocean, Prog. Oceanogr. 31:181-224, 1993 .

Mysak L. A., Generation of annual Rossby waves in North Pacific, Journal of Physical Oceanography, 13, 1908-1923, 1983.

Perigaud, C., and P. Delecluse, Annual sea level variations in the south tropical Indian Ocean from Geosat and shallow -water simulations, J. Geophys. Res., 97, 20169-20178, 1992.

Polito, P.S., Peter Cornillon, Long barocilinic Rossby waves detected by Topex/Poseidon, J. Geophys. Res., 102, 3,215-3,235, 1997.

Polito, P. S., O. T. Sato, and W. T. Liu, Characterization and validation of the heat storage variability from TOPEX/POSEIDON at four oceanographic sites, Journal of Geophysical Research., Vol. 105, No. C7, 2000.

Potemra, J. T., M. E. Luther, The seasonal circulation of the upper ocean in the Bay of Bengal', J. Geophys. Res., 96, 12,667-12,683,1991.

Quartly, G. D., P. Cipollini and P. G. Challenor, Synergistic observation of Rossby waves', proceeding of ERS – ENVISAT symposium, 16-20th October, Gothenburg, (Sweden), 2000.

Reddy, P. R. C., P. S. Salvekar, A. A. Deo, and D. W. Ganer, Westward propagating twin gyres in the equatorial Indian Ocean', J. Geophys. Letter, vol. 31, doi:10.1027/2003Gl018615, 2004.

Rao, S. A., S. K. Behera, Y. Masumoto and T. Yamagata, Interannual surface variability in the tropical Indian Ocean with special emphasis on Indain Ocean Dipole, Deep Sea Res. II, 49, 1549 – 1572, 2002.

Saji N. H., B. N. Gosawami P. N. Vinyachandran and T. Yamagata, A dipole mode in the tropical Indian Ocean', Nature, 401, 360-363, 1999.

Schlax. M. G., and D. B. Chelton, Aliased tidal errors in Topex/Poseidon sea surface height data', J. Geophys. Res. 99, 24,761-24,775, 1994.

Shenoi, S. S. C., D. Shankar, and S. R. Shetye, On the sea surface temperature high in the Lakshadweep sea before the onset of the southwest monsoon, J. Geophys. Res. 104, 15703-15712, 1999.

Vinyachandran P. N., S. Iizuka and T. Yamagata, Indian Ocean dipole mode event in an ocean general circulation model', Deep Sea Res. II, 49, 1573 – 1596, 2002.

Yu, L., J. J. O'Brien and J. Yang, On the remote forcing of the circualetion in the Bay of Bengal, J. Geophys. Res. 96, 20,449-20,454, 1992.

Table A: is showing the mean phase speed, time period, wave length and amplitude of different components of the Rossby and Kelvin waves.

			Means Values				
Lat. +=N -=S	**Long. Range °E - °E**	**Filtered compo-nent**	**Phase speed Km/days**	**Time period Days**	**Wave-length Kms**	**Ampli-tude MM**	**Number of days***
-12.5	51.5-121.5	24	-11.55	539	-6198	15	674
-12.5	51.5-121.5	12	-12.9	331	-4272	29	604
-12.5	51.5-121.5	6	-6.18	168	-2701	19	481
-12.5	51.5-121.5	3	-15	86	-1320	28	502
-12.5	51.5-121.5	1	-13.07	54	-699	32	596
-8.5	40.5-114.5	24	-12.1	662	-8014	14	680
-8.5	40.5-114.5	12	-18.95	331	-6194	13	434
-8.5	40.5-114.5	6	-12.27	292	-3584	25	671
-8.5	40.5-114.5	3	-3365	82	-2728	8	244
-8.5	40.5-114.5	1	-15.95	67	-1043	25	516
-5.5	40.5-103.5	12	-22.52	370	-8285	11	311
-5.5	40.5-103.5	6	-58.63	155	-9065	16	119
-5.5	40.5-103.5	3	-52.04	88	-4515	20	134
-5.5	40.5-103.5	1	-28.79	56	-1546	31	243
-0.5	43.5-97.5	24	-24.05	620	-14906	3	250
-0.5	43.5-97.5	12	-31.94	233	-7475	9	193
-0.5	43.5-97.5	6	-51.72	153	-7858	5	117
-0.5	43.5-97.5	3	-37.18	97	-3538	6	162
-0.5	43.5-97.5	1	-25.01	52	-1273	9	240
0.5	44.5-96.5	24	-20.72	660	-13666	3	289
0.5	44.5-96.5	12	-31.72	253	-8041	8	186
0.5	44.5-96.5	6	-48.4	162	-7848	4	120
0.5	44.5-96.5	3	-38.03	92	-3457	5	152
0.5	44.5-96.5	1	-2493	53	-1309	8	241
5.5	49.5-76.5	12	-30.55	258	-7512	12	100
5.5	49.5-76.5	6	-44.12	136	-5934	23	68

Table A Continued

5.5	49.5-76.5	3	-67.3	80	-5341	3	44
5.5	49.5-76.5	1	-29.15	48	-1358	35	103
8.5	51.5-76.5	12	-23.31	235	-5483	14	116
8.5	51.5-76.5	6	-31.99	149	-4735	15	86
8.5	51.5-76.5	3	-35.67	88	-2977	9	76
12.5	55.5-73.5	12	-6.77	362	-2449	16	295
12.5	55.5-73.5	6	-73.25	130	-9388	12	27
12.5	55.5-73.5	3	-15.31	88	-1311	23	103

Here 24 = Biannual Rossby Wave component, 12= Annual Rossby wave component, 6 = Semi annual Rossby Wave component, 3 = Trimestral Rossby wave component 1 = Monthly Rossby wave component OR Tropical instability waves

And * = mean no. of days taken by the Rossby waves components to cross longitudinal distance at that latitude.

Negative sign of phase speed means the westward propagation of wave component

Table B: Latitudinal thresholds for each wave band and basin.

Band	Latitudinal extend
η_{24}	52.5°S, 17.5°N
η_{12}	47.5°S, 17.5°N
η_{6}	39.5°S, 17.5°N
η_{3}	23.5°S, 17.5°N
η_{1}	13.5°S, 17.5°N
Kelvin	5.5°S, 5.5°N

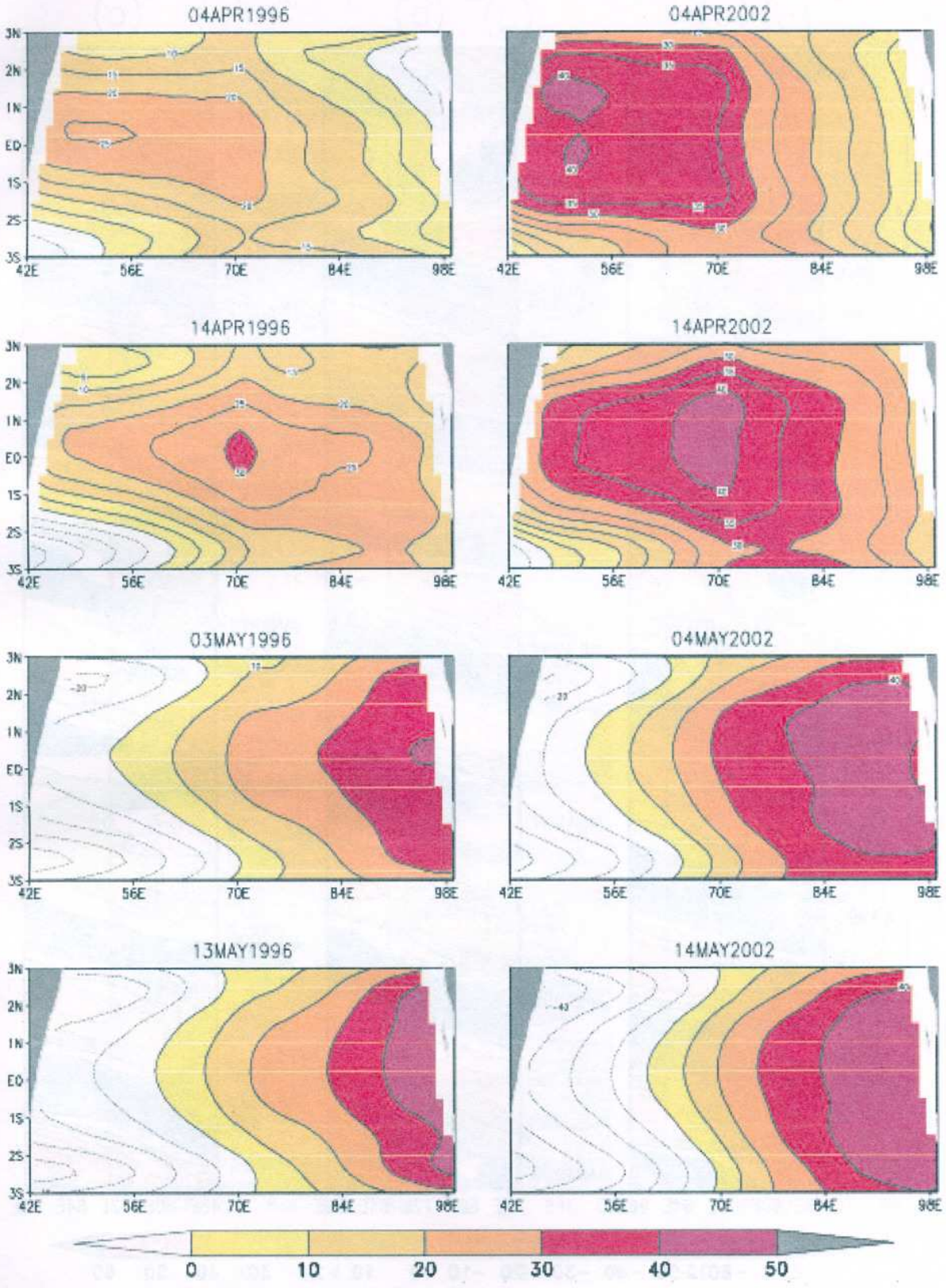

Fig 1: Propagation of semi annual K. waves (mm) 1996 (left panel) and 2002 (right panel).

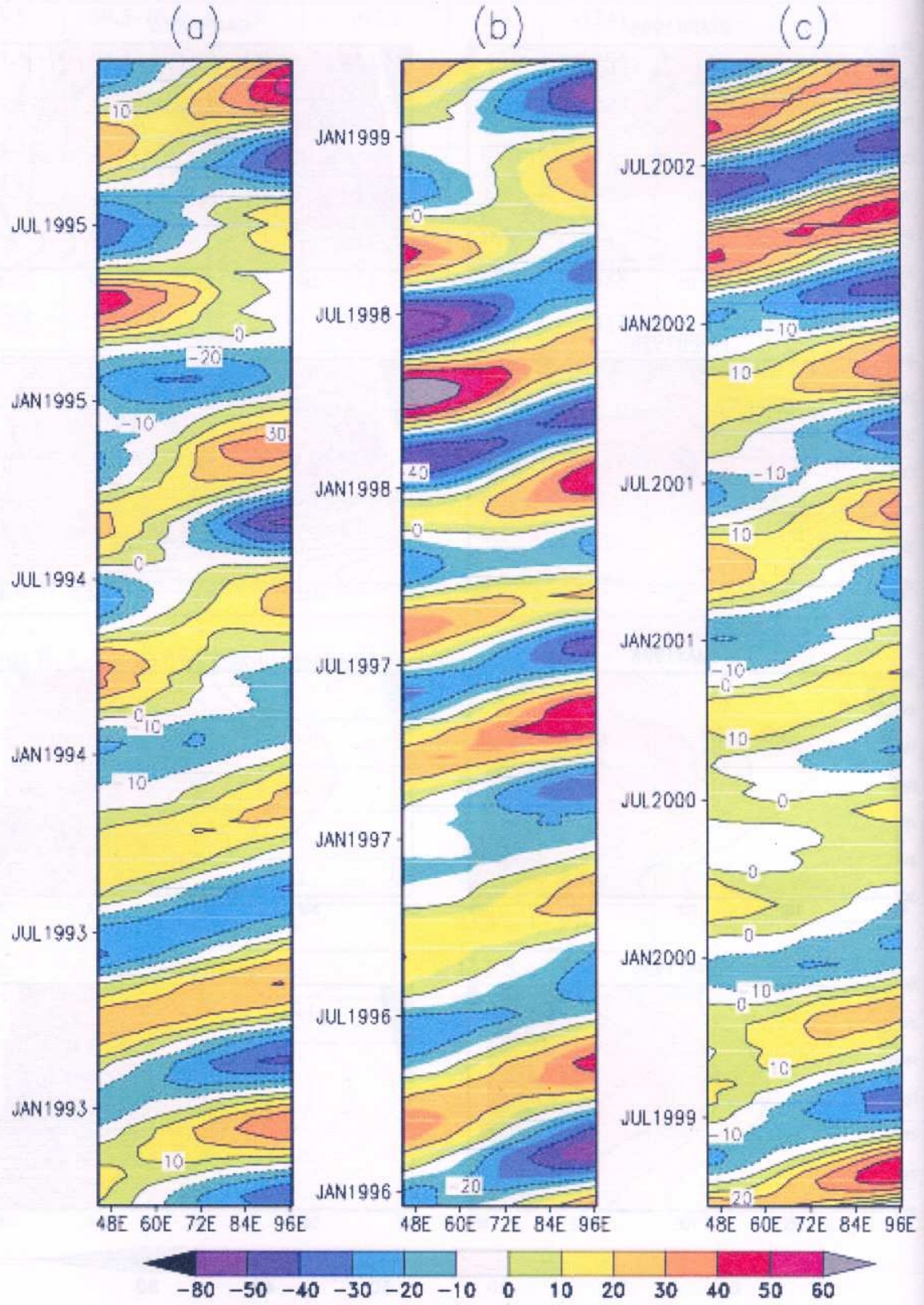

Fig 2: Longitude-Time plot of Semi annual Kelvin waves (mm) along Equator; Cycles (a) 1-120 (b) 120-240 (c) 240-373.

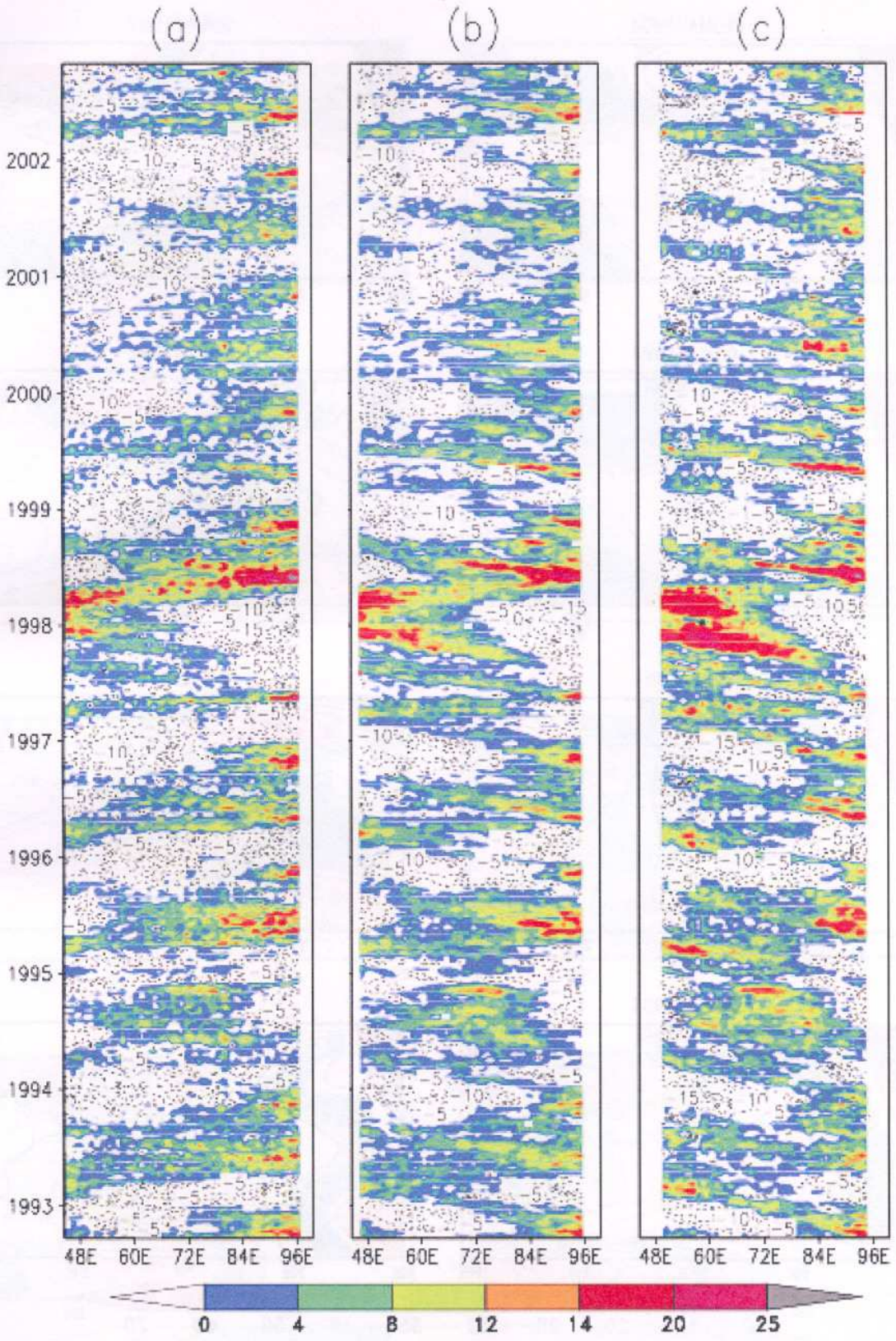

Fig 3: Longitude-Time plot of Topex (cm) (a) along Equator (b) average of 2.5N and 2.5S (c) average of 4.5N and 4.5S..

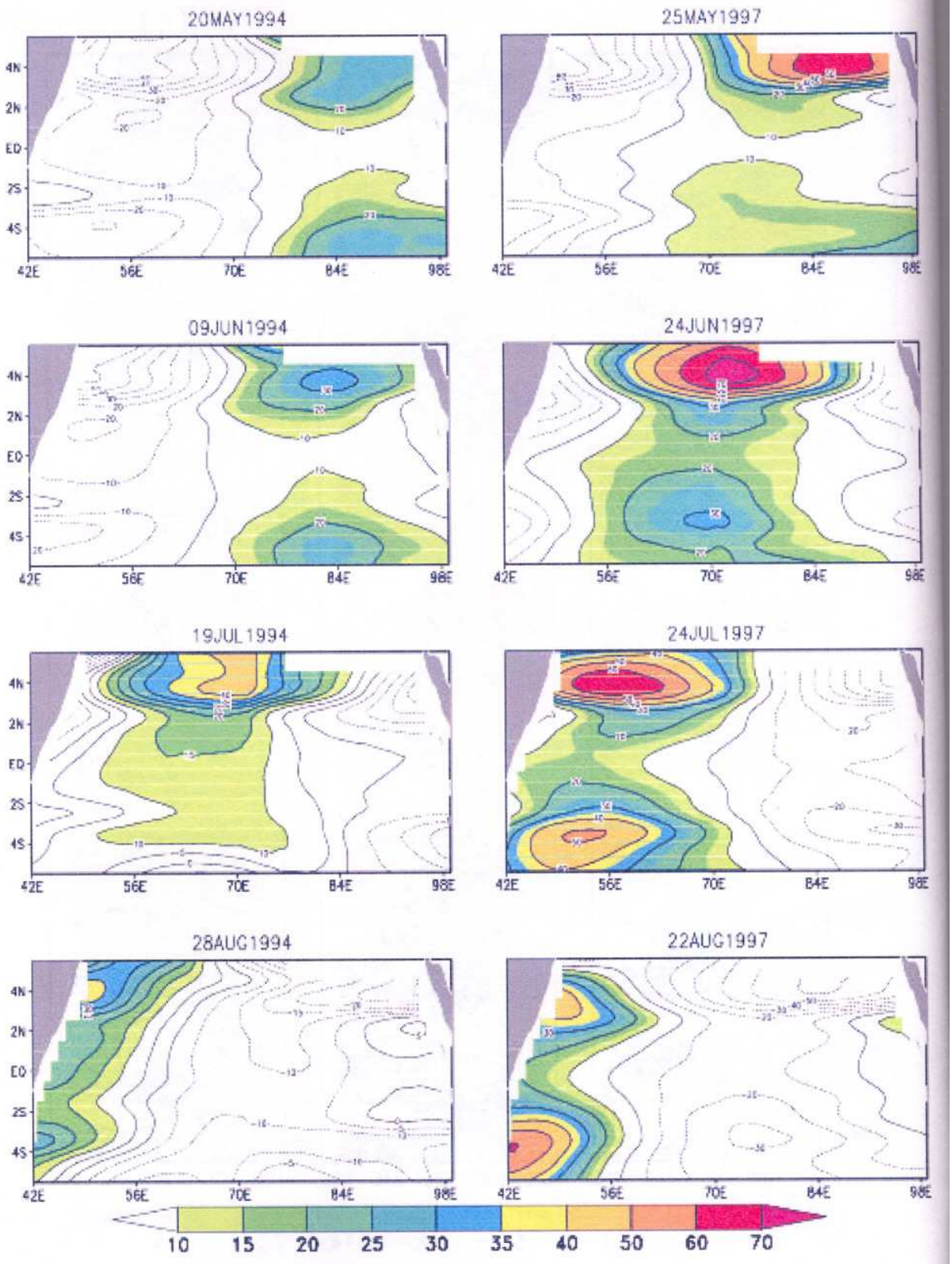

Fig 4: Propagation of semi annual Rossby waves (mm) 1994 (left panel) and 1997 (right panel).

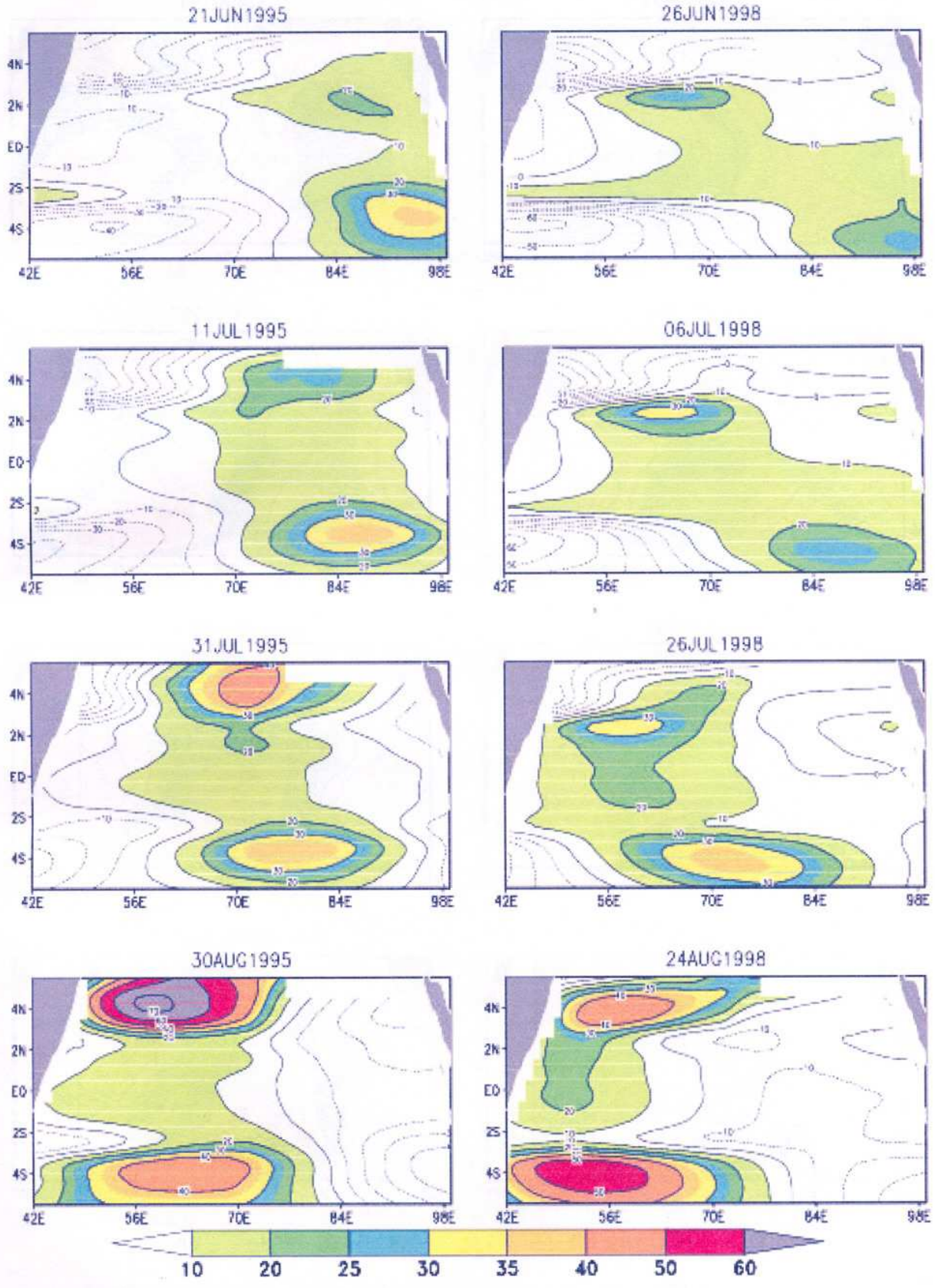

Fig 5: Propagation of semi Annual R. waves (mm) 1995 (left panel) and 1998 (right panel)

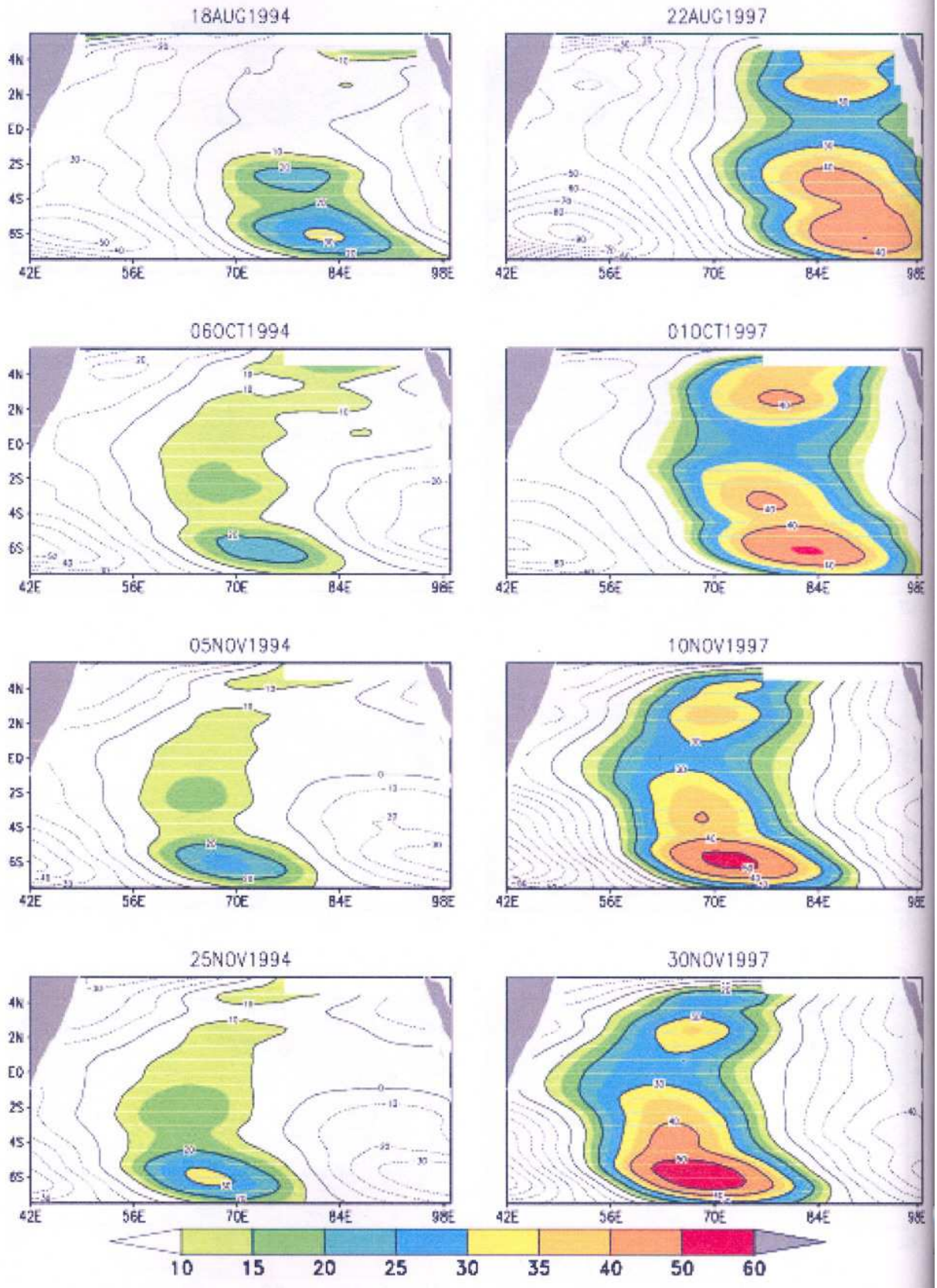

Fig 6: Propagation of Annual Rossby waves (mm)1994 (left panel) and 1997 (right panel)

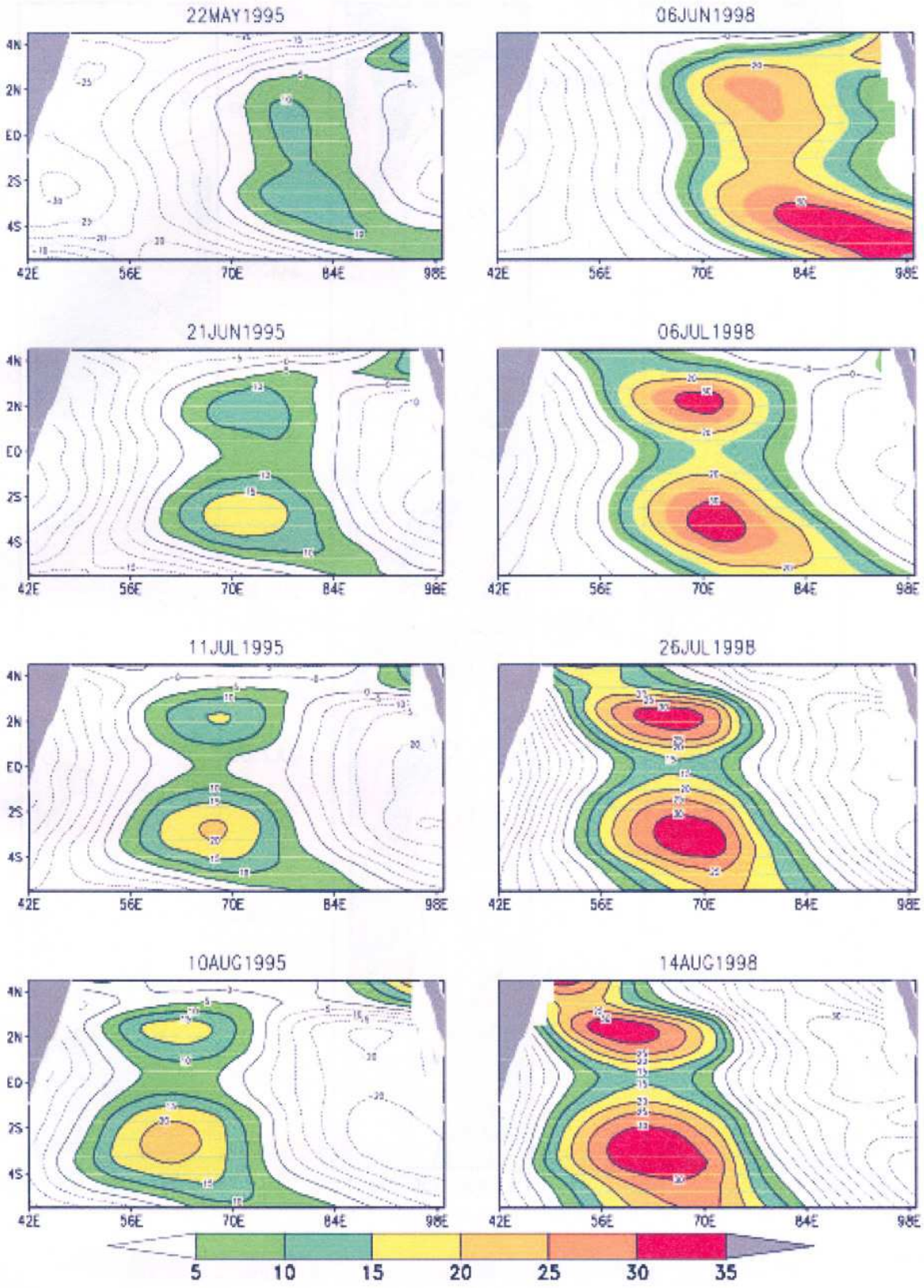

Fig 7: Propagation of Annual R. waves (mm) 1995 (left panel) and 1998 (right panel)

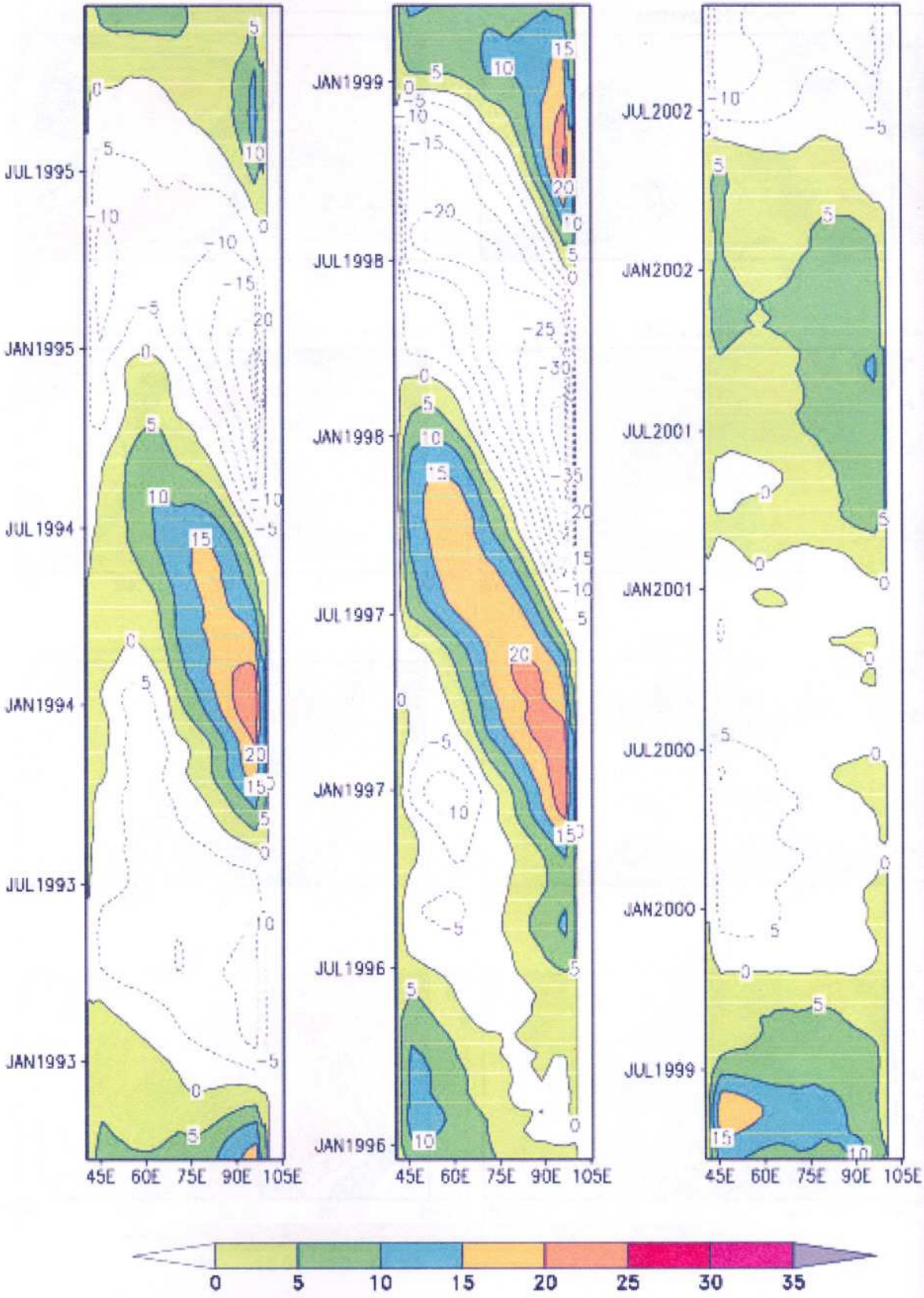

Fig 8: Propagation of Biannual Rossby waves (mm) average of 1.5N to 3.5S.

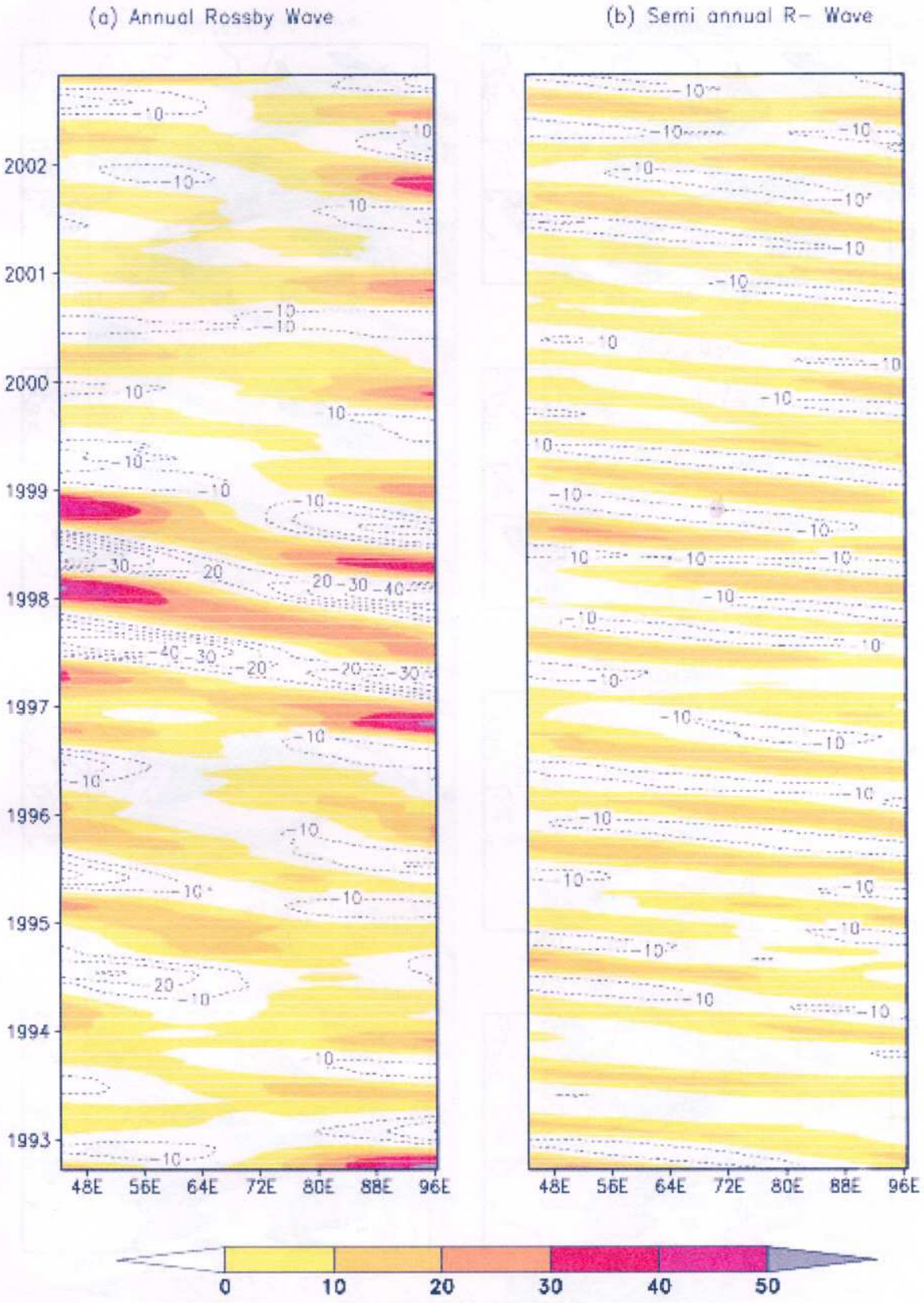

Fig 9: Propagation of Annual and semi Annual R. waves (mm) here average of 4.5N to 4.5S.

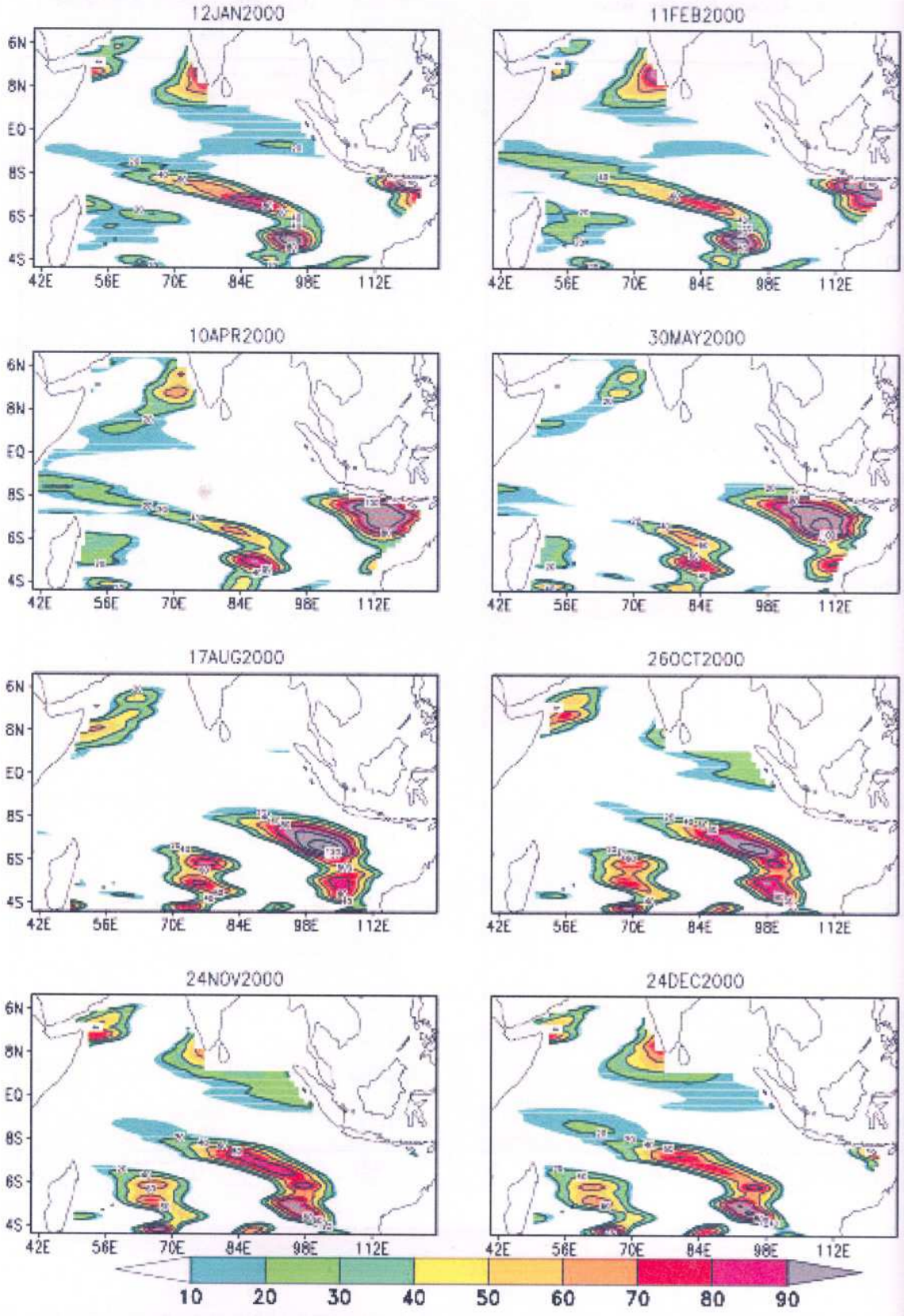

Fig 10: Propagation of Annual Rossby waves (mm) in 2000.

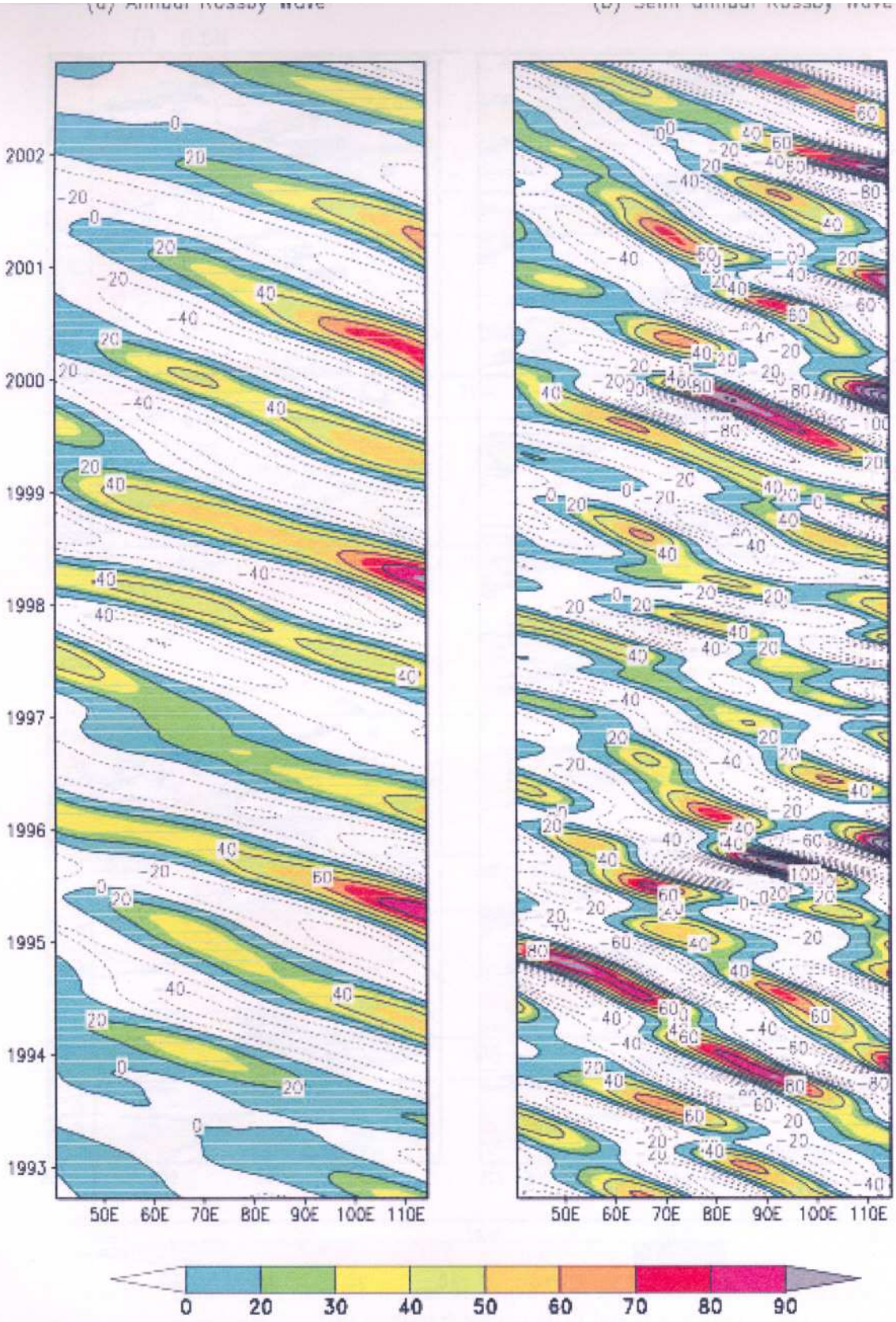

Fig 11: Propagation of Annual and semi Annual Rossby waves (mm) along 8.5S.

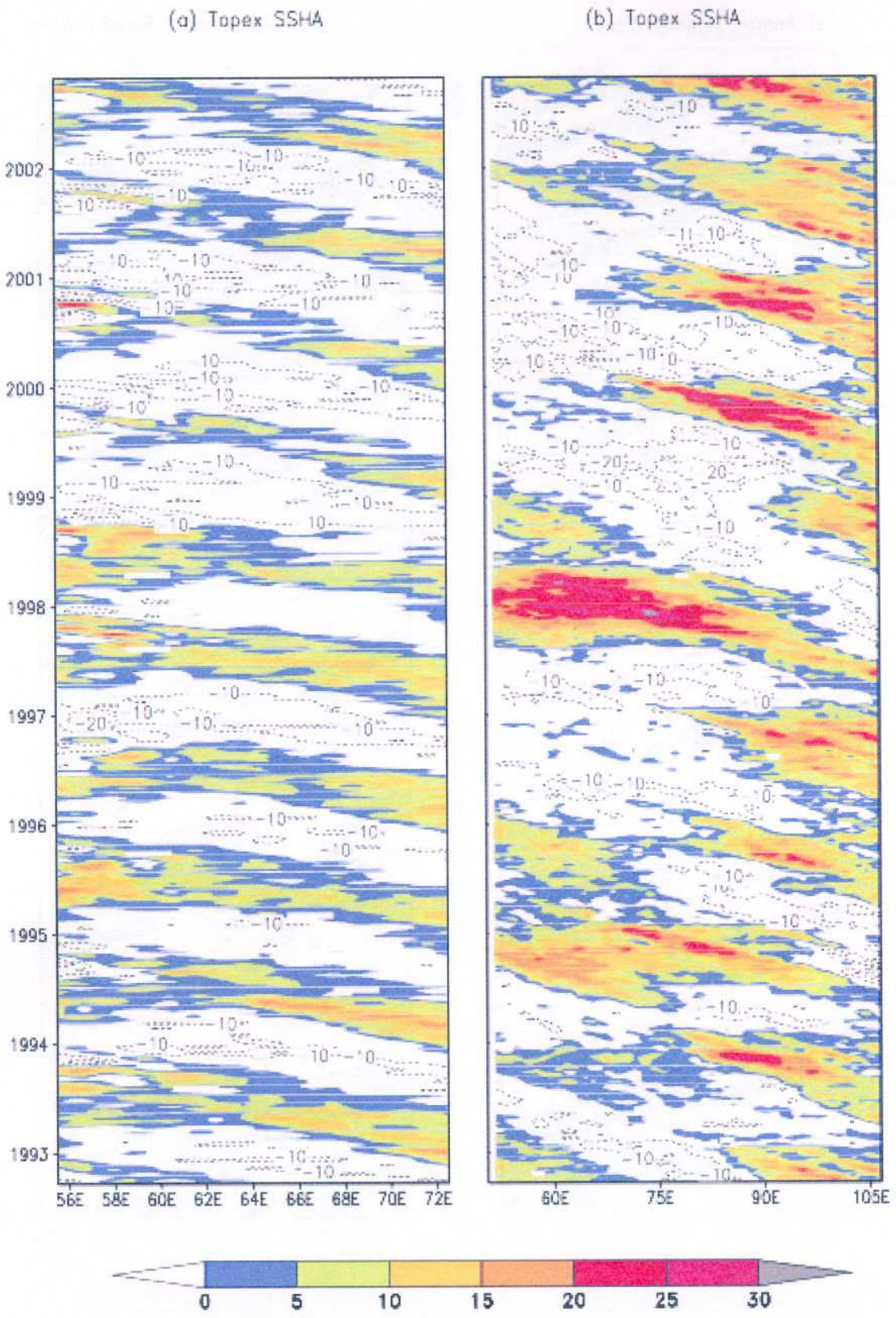

Fig 12 : (a) average from 10.5N to 14.5N (b) average from 7.5S to 12.5S in cm.

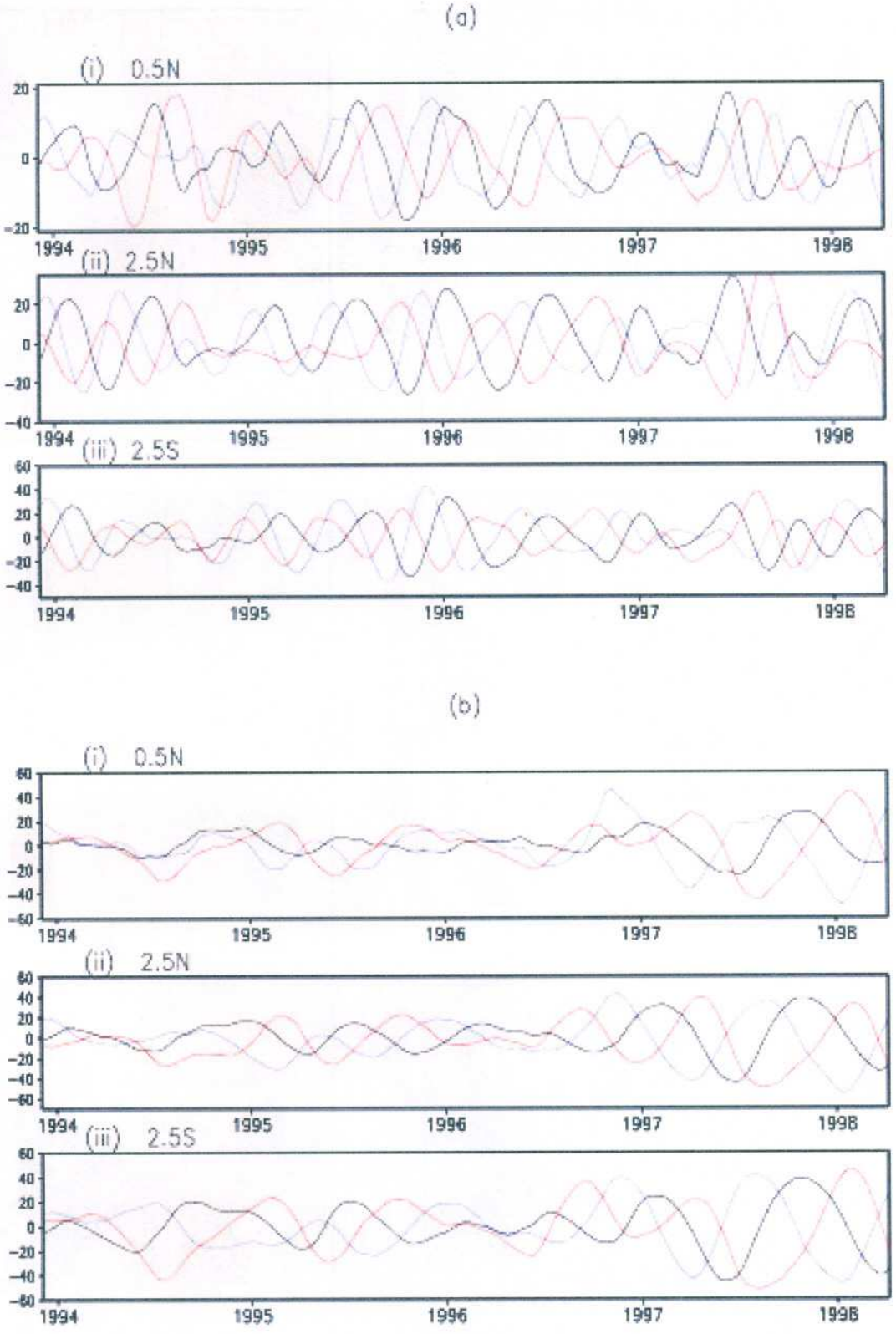

Fig 13 : Time series of semi annual R. waves [(a) top three panel] and annual Rossby waves [(b) bottom three panel] at lon. 90E (blue), 70E (black) and 50E (red) on lat. 0.5N, 2.5N and 2.5S.

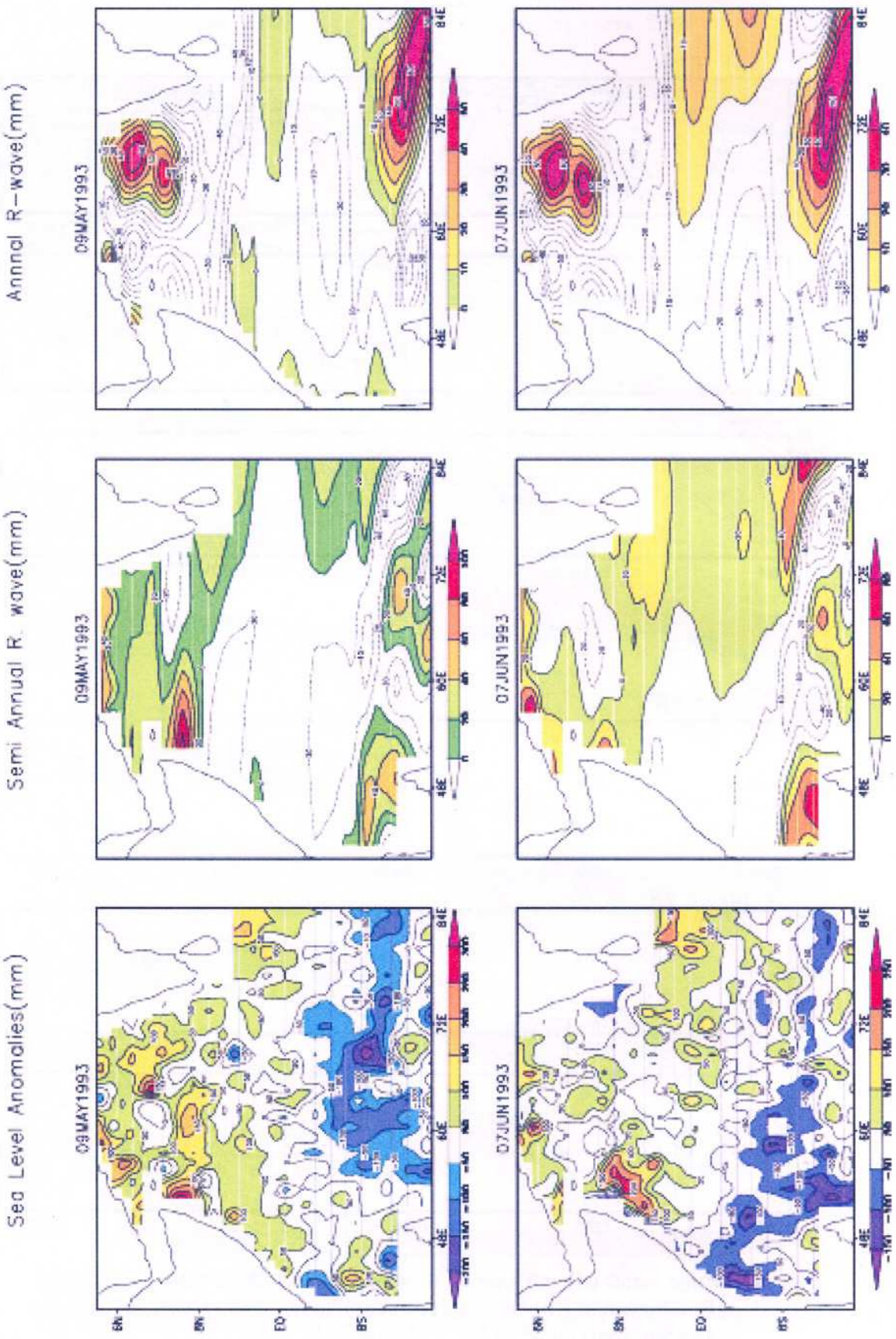

Fig 14a : Seasonal fluctuation in Sea level Anomalies.

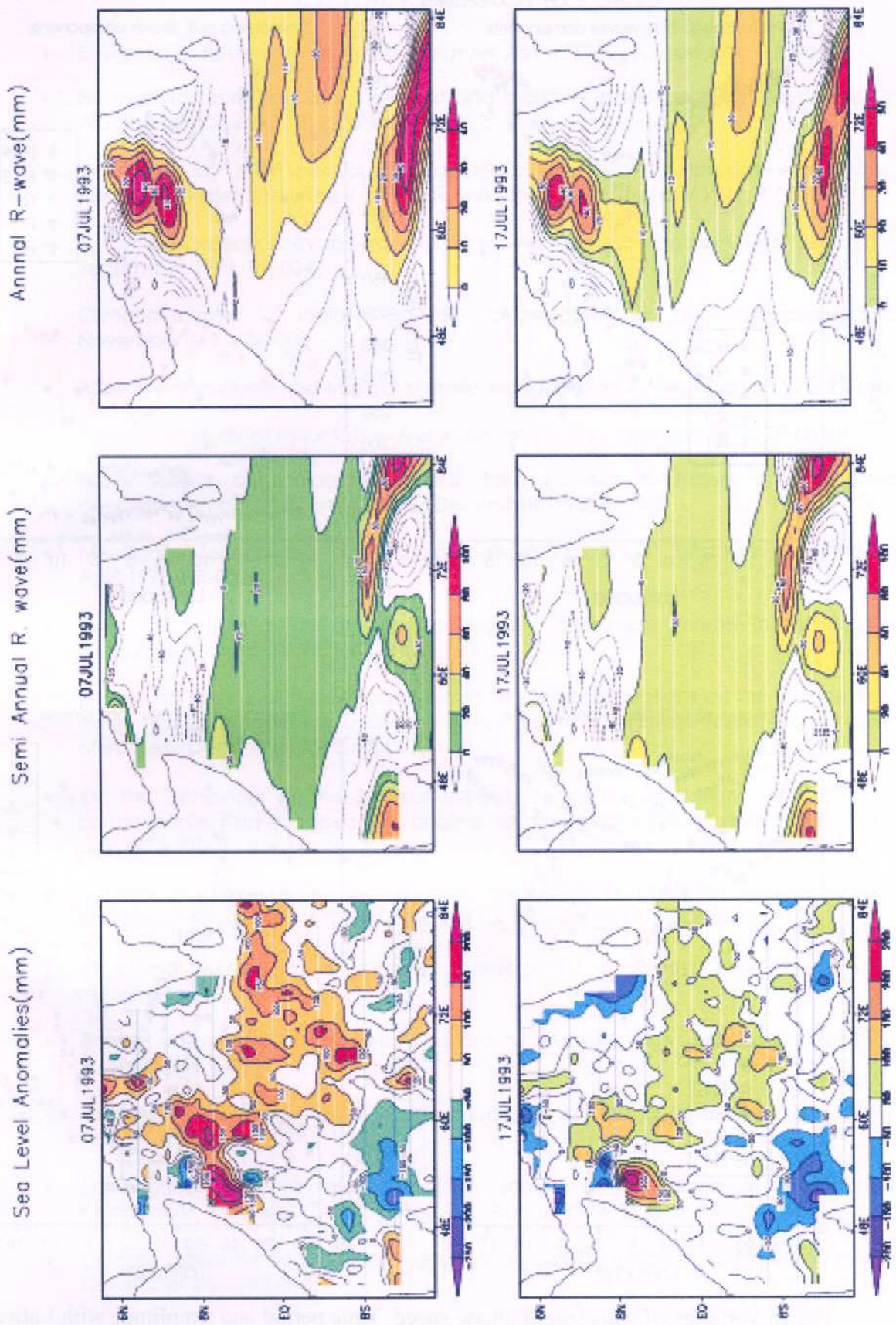

Fig 14b : Seasonal fluctuation in Sea level Anomalies.

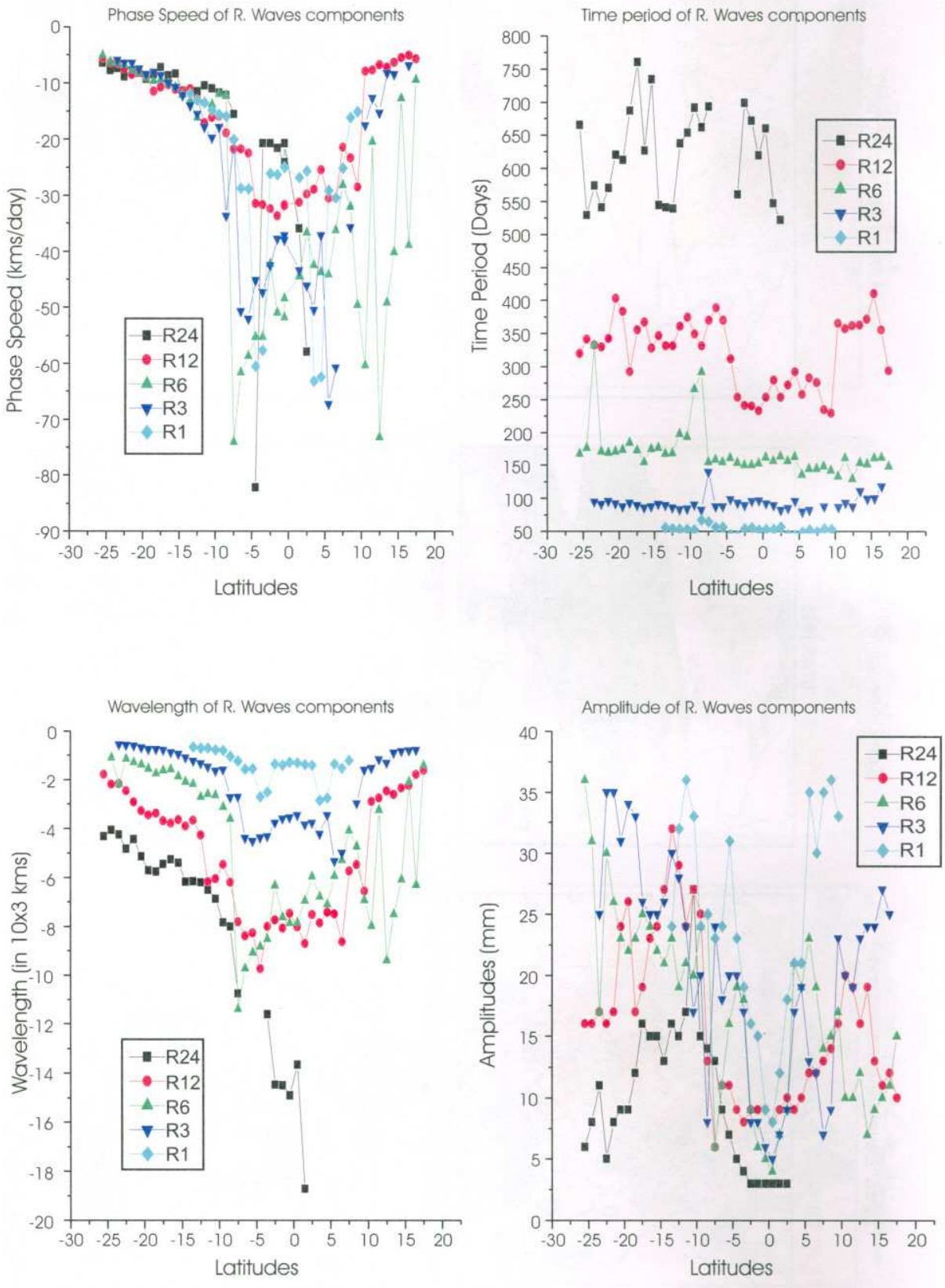

Fig 15:Variation of wavelength, Phase speed, Time period and Amplitude with Latitudes

I. I. T. M. RESEARCH REPORTS

- Energetic consistency of truncated models, *Asnani G.C.*, August 1971, RR-001.
- Note on the turbulent fluxes of heat and moisture in the boundary layer over the Arabian Sea, *Sinha S.*, August 1971, RR-002.
- Simulation of the spectral characteristics of the lower atmosphere by a simple electrical model and using it for prediction, *Sinha S.*, September 1971, RR-003.
- Study of potential evapo-transpiration over Andhra Pradesh, *Rakhecha P.R.*, September 1971, RR-004.
- Climatic cycles in India-1: Rainfall, *Jagannathan P. and Parthasarathy B.*, November 1971, RR-005.
- Tibetan anticyclone and tropical easterly jet, *Raghavan K.*, September 1972, RR-006.
- Theoretical study of mountain waves in Assam, *De U.S.*, February 1973, RR-007.
- Local fallout of radioactive debris from nuclear explosion in a monsoon atmosphere, *Saha K.R. and Sinha S.*, December 1972, RR-008.
- Mechanism for growth of tropical disturbances, *Asnani G.C. and Keshavamurty R.N.*, April 1973, RR-009.
- Note on "Applicability of quasi-geostrophic barotropic model in the tropics", *Asnani G.C.*, February 1973, RR-010.
- On the behaviour of the 24-hour pressure tendency oscillations on the surface of the earth, Part-I: Frequency analysis, Part-II: Spectrum analysis for tropical stations, *Misra B.M.*, December 1973, RR-011.
- On the behaviour of the 24 hour pressure tendency oscillations on the surface of the earth, Part-III : Spectrum analysis for the extra-tropical stations, *Misra B.M.*, July 1976, RR-011A.
- Dynamical parameters derived from analytical functions representing Indian monsoon flow, *Awade S.T. and Asnani G.C.*, November 1973, RR-012.
- Meridional circulation in summer monsoon of Southeast Asia, *Asnani G.C.*, November 1973, RR-014.
- Energy conversions during weak monsoon, *Keshavamurty R.N. and Awade S.T.*, August 1974, RR-015.
- Vertical motion in the Indian summer monsoon, *Awade S.T. and Keshavamurty R.N.*, August 1974, RR-016.
- Semi-annual pressure oscillation from sea level to 100mb in the northern hemisphere, *Asnani G.C. and Verma R.K.*, August 1974, RR-017.
- Suitable tables for application of gamma probability model to rainfall, *Mooley D.A.*, November 1974, RR-018.
- Annual and semi-annual thickness oscillation in thenorthern hemisphere, *Asnani G.C. and Verma R.K.*, January 1975, RR-020.

- Spherical harmonic analysis of the normal constant pressure charts in the northern hemisphere, *Awade S.T., Asnani G.C. and Keshavamurty R.N.*, May 1978, RR-021.

- Dynamical parameters derived from analytical function representing normal July zonal flow along 87.5 °E, *Awade S.T. and Asnani G.C.*, May 1978, RR-022.

- Study of trends and periodicities in the seasonal and annual rainfall of India, *Parthasarathy B. and Dhar O.N.*, July 1975, RR-023.

- Southern hemisphere influence on Indian rainfall, *Raghavan K.., Paul D.K. and Upasani P.U.*, February 1976, RR-024.

- Climatic fluctuations over Indian region - Rainfall : A review, *Parthasarathy B. and Dhar O.N.*, May 1978, RR-025.

- Annual variation of meridional flux of sensible heat, *Verma R.K. and Asnani G.C.*, December 1978, RR-026.

- Poisson distribution and years of bad monsoon over India, *Mooley D.A and Parthasarathy B.*, April 1980, RR-027.

- On accelerating the FFT of Cooley and Tukey, *Mishra S.K.*, February 1981, RR-028.

- Wind tunnel for simulation studies of the atmospheric boundary layer, *Sivaramakrishnan S.*, February 1981, RR-029.

- Hundred years of Karnataka rainfall, *Parthasarathy B. and Mooley D.A.*, March 1981, RR-030.

- Study of the anomalous thermal and wind patterns during early summer season of 1979 over the Afro-Asian region in relation to the large-scale performance of the monsoon over India, *Verma R.K. and Sikka D.R.*, March 1981, RR-031.

- Some aspects of oceanic ITCZ and its disturbances during the onset and established phase of summer monsoon studied with Monex-79 data, *Sikka D.R., Paul D.K. and Singh S.V.*, March 1981, RR- 032.

- Modification of Palmer drought index, *Bhalme H.N. and Mooley D.A.*, March 1981, RR-033.

- Meteorological rocket payload for Menaka-II/Rohini 200 and its developmental details, *Vernekar K.G. and Brij Mohan*, April 1981, RR-034.

- Harmonic analysis of normal pentad rainfall of Indian stations, *Anathakrishnan R. and Pathan J.M.*, October 1981, RR-035.

- Pentad rainfall charts and space-time variations of rainfall over India and the adjoining areas, *Anathakrishnan R. and Pathan J.M.*, November 1981, RR-036.

- Dynamic effects of orography on the large scale motion of the atmosphere Part I : Zonal flow and elliptic barrier with maximum height of one km., *Bavadekar S.N. and Khaladkar R.M.*, January 1983, RR-037.

- Limited area five level primitive equation model, *Singh S.S.*, February 1983, RR-038.

- Developmental details of vortex and other aircraft thermometers, *Vernekar K.G., Brij Mohan and Srivastava S.*, November 1983, RR-039.

- Note on the preliminary results of integration of a five level P.E. model with westerly wind and low orography, *Bavadekar S.N., Khaladkar R.M., Bandyopadhyay A. and Seetaramayya P.*, November 1983, RR-040.

- Long-term variability of summer monsoon and climatic change, *Verma R.K., Subramaniam K. and Dugam S.S.*, December 1984, RR-041.

- Project report on multidimensional initialization for NWP models, *Sinha S.*, February 1989, RR-042.

- Numerical experiments with inclusion of orography in five level P.E. Model in pressure-coordinates for interhemispheric region, *Bavadekar S.N. and Khaladkar R.M.*, March 1989, RR-043.

- Application of a quasi-lagrangian regional model for monsoon prediction, *Singh S.S. and Bandyopadhyay A.*, July 1990, RR-044.

- High resolution UV-visible spectrometer for atmospheric studies, *Bose S., Trimbake H.N., Londhe A.L. and Jadhav D.B.*, January 1991, RR-045.

- Fortran-77algorithm for cubic spline interpolation for regular and irregular grids, *Tandon M.K.*, November 1991, RR-046.

- Fortran algorithm for 2-dimensional harmonic analysis, *Tandon M.K.*, November 1991, RR- 047.

- 500 hPa ridge and Indian summer monsoon rainfall : A detailed diagnostic study, *Krishna Kumar K., Rupa Kumar K. and Pant G.B.*, November 1991, RR-048.

- Documentation of the regional six level primitive equation model, *Singh S.S. and Vaidya S.S.*, February 1992, RR-049.

- Utilisation of magnetic tapes on ND-560 computer system, *Kripalani R.H. and Athale S.U.*, July 1992, RR-050.

- Spatial patterns of Indian summer monsoon rainfall for the period 1871-1990, *Kripalani R.H., Kulkarni A.A., Panchawagh N.V. and Singh S.V.*, August 1992, RR-051.

- FORTRAN algorithm for divergent and rotational wind fields, *Tandon M.K.*, November 1992, RR-052.

- Construction and analysis of all-India summer monsoon rainfall series for the longest instrumental period: 1813-1991, *Sontakke N.A., Pant G.B. and Singh N.*, October 1992, RR-053.

- Some aspects of solar radiation, *Tandon M.K.*, February 1993, RR-054.

- Design of a stepper motor driver circuit for use in the moving platform, *Dharmaraj T. and Vernekar K.G.*, July 1993, RR-055.

- Experimental set-up to estimate the heat budget near the land surface interface, *Vernekar K.G., Saxena S., Pillai J.S., Murthy B.S., Dharmaraj T. and Brij Mohan*, July 1993, RR-056.

- Identification of self-organized criticality in atmospheric total ozone variability, *Selvam A.M. and Radhamani M.*, July 1993, RR-057.

- Deterministic chaos and numerical weather prediction, *Selvam A.M.*, February 1994, RR-058.

- Evaluation of a limited area model forecasts, *Singh S.S., Vaidya S.S Bandyopadhyay A., Kulkarni A.A, Bawiskar S.M.,Sanjay J., Trivedi D.K. and Iyer U.*, October 1994, RR-059.

- Signatures of a universal spectrum for atmospheric interannual variability in COADS temperature time series, *Selvam A.M., Joshi R.R. and Vijayakumar R.*, October 1994, RR-060.

- Identification of self-organized criticality in the interannual veriability of global surface temperature, *Selvam A.M. and Radhamani M.*, October 1994, RR-061.

- Identification of a universal spectrum for nonlinear veriability of solar-geophysical parameters, *Selvam A.M., Kulkarni M.K., Pethkar J.S. and Vijayakumar R.*, October 1994, RR-062.

- Universal spectrum for fluxes of energetic charged particles from the earth's magnetosphere, *Selvam A.M. and Radhamani M.*, June 1995, RR-063.

- Estimation of nonlinear kinetic energy exchanges into individual triad interactions in the frequency domain by use of the cross-spectral technique, *Chakraborty D.R.*, August 1995, RR-064.

- Monthly and seasonal rainfall series for all-India homogeneous regions and meteorological subdivisions: 1871-1994, *Parthasarathy B., Munot A.A. and Kothawale D.R.*, August 1995, RR-065.

- Thermodynamics of the mixing processes in the atmospheric boundary layer over Pune during summer monsoon season, *Morwal S.B. and Parasnis S.S.*, March 1996, RR-066.

- Instrumental period rainfall series of the Indian region: A documentation, *Singh N. and Sontakke N.A.*, March 1996, RR-067.

- Some numerical experiments on roundoff-error growth in finite precision numerical computation, *Fadnavis S.*, May 1996, RR-068.

- Fractal nature of MONTBLEX time series data, *Selvam A.M. and Sapre V.V.*, May 1996, RR-069.

- Homogeneous regional summer monsoon rainfall over India: Interannual variability and teleconnections, *Parthasarathy B., Rupa Kumar K. and Munot A.A.*, May 1996, RR-070.

- Universal spectrum for sunspot number variability, *Selvam A.M. and Radhamani M.*, November 1996, RR-071.

- Development of simple reduced gravity ocean model for the study of upper north Indian ocean, *Behera S.K. and Salvekar P.S.*, November 1996, RR-072.

- Study of circadian rhythm and meteorological factors influencing acute myocardial infraction, *Selvam A.M., Sen D. and Mody S.M.S.*, April 1997, RR-073.

- Signatures of universal spectrum for atmospheric gravity waves in southern oscillation index time series, *Selvam A.M., Kulkarni M.K., Pethkar J.S. and Vijayakumar R.*, December 1997, RR-074.

- Some example of X-Y plots on Silicon Graphics, *Selvam A.M., Fadnavis S. and Gharge S.P.*, May 1998, RR-075.

- Simulation of monsoon transient disturbances in a GCM, *Ashok K., Soman M.K. and Satyan V.*,August 1998, RR-076.

- Universal spectrum for intraseasonal variability in TOGA temperature time series, *Selvam A.M., Radhamani M., Fadnavis S. and Tinmaker M.I.R.*, August 1998, RR-077.

- One dimensional model of atmospheric boundary layer, *Parasnis S.S., Kulkarni M.K., Arulraj S. and Vernekar K.G.*, February 1999, RR-078.

- Diagnostic model of the surface boundary layer - A new approach, *Sinha S.*, February 1999, RR-079.

- Computation of thermal properties of surface soil from energy balance equation using force - restore method, *Sinha S.*, February 1999, RR-080.

- Fractal nature of TOGA temperature time series, *Selvam A.M. and Sapre V.V.*, February 1999, RR-081.

- Evolution of convective boundary layer over the Deccan Plateau during summer monsoon, *Parasnis S.S.*, February 1999, RR-082.

- Self-organized criticality in daily incidence of acute myocardial infarction, *Selvam A.M., Sen D., and Mody S.M.S.*, Feburary 1999, RR-083.

- Monsoon simulation of 1991 and 1994 by GCM : Sensitivity to SST distribution, *Ashrit R.G., Mandke S.K. and Soman M.K.*, March 1999, RR-084.

- Numerical investigation on wind induced interannual variability of the north Indian Ocean SST, *Behera S.K., Salvekar P.S. and Ganer D.W.*, April 1999, RR-085.

- On step mountain eta model, *Mukhopadhyay P., Vaidya S.S., Sanjay J. and Singh S.S.*, October 1999, RR-086.

- Land surface processes experiment in the Sabarmati river basin: an overview and early results, *Vernekar K.G., Sinha S., Sadani L.K., Sivaramakrishnan S., Parasnis S.S., Brij Mohan, Saxena S., Dharamraj T., Pillai, J.S., Murthy B.S., Debaje, S.B., Patil, M.N. and Singh A.B.*, November 1999, RR-087.

- Reduction of AGCM systematic error by Artificial Neural Network: A new approach for dynamical seasonal prediction of Indian summer monsoon rainfall, *Sahai A.K. and Satyan V.*, December 2000, RR-088.

- Ensemble GCM simulations of the contrasting Indian summer monsoons of the 1987 and 1988, *Mujumdar M.* and *Krishnan R.*, February 2001, RR-089.

- Aerosol measurements using lidar and radiometers at Pune during INDOEX field phases, *Maheskumar R.S., Devara P.C.S., Raj P.E., Jaya Rao Y.,Pandithurai G., Dani K.K., Saha S.K., Sonbawne S.M. and Tiwari Y.K.*, December 2001, RR-090.

- Modelling studies of the 2000 Indian summer monsoon and extended analysis, *Krishnan R., Mujumdar M., Vaidya V., Ramesh K.V. and Satyan V.*, December 2001, RR-091.

- Intercomparison of Asian summer monsoon 1997 simulated by atmospheric general circulation models, *Mandke S.K., Ramesh K.V. and Satyan V.*, December 2001, RR-092.

- Prospects of prediction of Indian summer monsoon rainfall using global SST anomalies, *Sahai A.K, Grimm A.M., Satyan V. and Pant G.B.*, April 2002, RR-093.

- Estimation of nonlinear heat and momentum transfer in the frequency domain buy the use of frequency co-spectra and cross-bispectra, *Chakraborty D.R. and Biswas M.K.*, August 2002, RR-094

- Real time simulations of surface circulations by a simple ocean model, *P Rahul Chand Reddy, Salvekar P.S., Ganer D.W. and Deo A.A.*, January 2003, RR-095

- Evidence of twin gyres in the Indian ocean : new insights using reduced gravity model by daily winds, *P Rahul Chand Reddy, Salvekar P.S., Ganer D.W. and Deo A.A.*, February 2003, RR-096

- Dynamical seasonal prediction experiments of the Indian summer monsoon, *Milind Mujumdar, R. Krishnan and V. Satyan*, June 2003, RR-097

- Thermodynamics and dynamics of the upper ocean mixed layer in the central and eastern Arabian sea, *C. Gnanaseelan, A.K. Mishra, Bijoy Thompson and P.S. Salvekar*, August 2003, RR-098

- Measurement of profiles and surface energy fluxes on the west coast of India at Vasco-Da-Gama, Goa during ARMEX 2002-03, *S. Sivaramakrishnan, B.S. Murthy, T. Dharmaraj, Cini Sukumaran and T. Rajitha Madhu Priya*, August 2003, RR-099

- Time-mean oceanic response and interannual variability in a global ocean GCM simulation, *K.V. Ramesh and R. Krishnan*, September 2003, RR-100

- Multimodel scheme for prediction of monthly rainfall over India, *J.R. Kulkarni, Savita G. Kulkarni, Yogesh Badhe, Sanjeev S. Tambe, Bhaskar D. Kulkarni and G.B. Pant*, December 2003, RR-101

- Mixed-layer and thermocline interactions associated with monsoonal forcing over the Arabian sea, *R. Krishnan and K.V. Ramesh*, January 2004, RR-102